www.elsevier.com/locate/sigpro

Image super-resolution: The techniques, applications, and future

Linwei Yue, Huanfeng Shen, Jie Li, Qiangqiang Yuan, Hongyan Zhang, Liangpei Zhang

PII: S0165-1684(16)30053-6
DOI: http://dx.doi.org/10.1016/j.sigpro.2016.05.002
Reference: SIGPRO6122

To appear in: *Signal Processing*

Received date: 8 October 2015
Revised date: 1 March 2016
Accepted date: 1 May 2016

Cite this article as: Linwei Yue, Huanfeng Shen, Jie Li, Qiangqiang Yuan, Hongyan Zhang and Liangpei Zhang, Image super-resolution: The techniques applications, and future, *Signal Processing* http://dx.doi.org/10.1016/j.sigpro.2016.05.002

Image super-resolution: the techniques, applications, and future

Linwei Yue[1], Huanfeng Shen[2,3*], Jie Li[1], Qiangqiang Yuan[3,4], Hongyan Zhang[1,3], Liangpei Zhang[1,3*]

[1]The State Key Laboratory of Information Engineering in Surveying, Mapping and Remote Sensing, Wuhan University, Wuhan, P. R. China

[2]School of Resource and Environmental Science, Wuhan University, Wuhan, P. R. China

[3]Collaborative Innovation Center of Geospatial Technology, Wuhan University, Wuhan, P. R. China

[4]School of Geodesy and Geomatics, Wuhan University, Wuhan, P. R. China

shenhf@whu.edu.cn

zlp62@whu.edu.cn

[*]Corresponding authors:

Abstract

Super-resolution (SR) technique reconstructs a higher-resolution image or sequence from the observed LR images. As SR has been developed for more than three decades, both multi-frame and single-frame SR have significant applications in our daily life. This paper aims to provide a review of SR from the perspective of techniques and applications, and especially the main contributions in recent years. Regularized SR methods are most commonly employed in the last decade. Technical details are discussed in this article, including reconstruction models, parameter selection methods, optimization algorithms and acceleration strategies. Moreover, an exhaustive summary of the current applications using SR techniques has been presented. Lastly, the article discusses the current obstacles for future research.

Keywords: Super resolution; resolution enhancement; regularized framework; applications.

1. Introduction

Image spatial resolution refers to the capability of the sensor to observe or measure the smallest object, which depends upon the pixel size. As two-dimensional signal records, digital images with a higher resolution are always desirable in most applications. Imaging techniques have been rapidly developed in the last decades, and the resolution has reached a new level. The question is therefore: are image resolution enhancement techniques still required?

The fact is, although the high-definition displays in recent years have reached a new level (e.g., 1080*1920 for HDTV, 3840*2160 for some ultra HDTV, and 2048*1536 for some mobile devices), the need for resolution enhancement cannot be ignored in many applications [1]. For instance, to guarantee the long-term stable operation of the recording devices, as well as the appropriate frame rate for dynamic scenes, digital surveillance products tend to sacrifice resolution to some degree. A similar situation exists in the remote sensing field: there is always a tradeoff between the spatial, spectral, and temporal resolutions. As for medical imaging, within each imaging modality, specific physical laws are in control, defining the meaning of noise and the sensitivity of the imaging process. How to extract 3D models of the human structure with high-resolution images while reducing the level of radiation still remains a challenge [2, 3].

Based on these facts, the current techniques cannot yet satisfy the demands. Resolution enhancement is therefore still necessary, especially in fields such as video

surveillance, medical diagnosis, and remote sensing applications. Considering the high cost and the limitations of resolution enhancement through "hardware" techniques, especially for large-scale imaging devices, signal processing methods, which are known as super-resolution (SR), have become a potential way to obtain high-resolution (HR) images. With SR methods, we can go beyond the limit of the low-resolution (LR) observations, rather than improving the hardware devices.

SR is a technique which reconstructs a higher-resolution image or sequence from the observed LR images. Technically, SR can be categorized as multi-frame or single-frame based on the input LR information [4-8]. If multiple images of the same scene with sub-pixel misalignment can be acquired, the complementary information between them can be utilized to reconstruct a higher-resolution image or image sequence, as Fig. 1 shows. However, multiple LR images may sometimes not be available for the reconstruction, and thus we need to recover the HR image using the limited LR information, which is defined as single-frame SR [9-12].

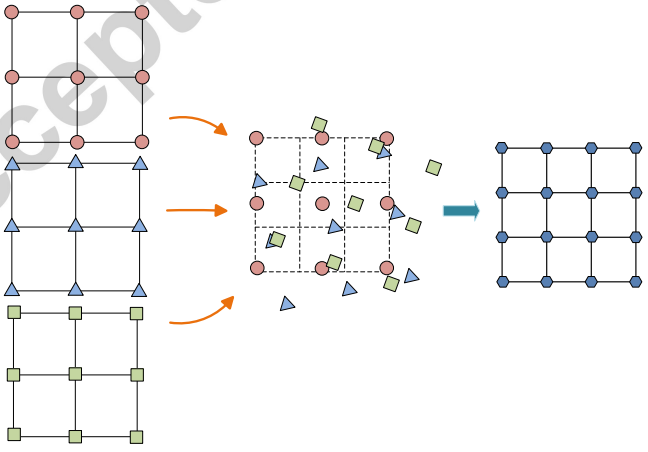

Fig. 1. The concept of multi-frame super-resolution. The grids on the left side represent the LR images of the same scene with sub-pixel alignment, thus the HR image (the grid on the right side) can be acquired by fusing the complementary information with SR methods.

Although SR techniques have been comprehensively summarized in several studies [4, 6, 8, 13-15], this paper aims to provide a review from the perspective of techniques and applications, and especially the main contributions in recent decades. This paper provides a more detailed description of the most commonly employed regularized SR methods, including fidelity models, regularization models, parameter estimation methods, optimization algorithms, acceleration strategies, etc. Moreover, we present an exhaustive summary of the current applications using SR techniques, such as the recent Google Skybox satellite application [16] and unmanned aerial vehicle (UAV) surveillance sequences [17]. The current obstacles for the future research are also discussed.

2. Technical background

Nowadays, charge-coupled devices (CCDs) and complementary metal oxide semiconductors (CMOSs) are the most widely used image sensors [4, 18]. To obtain an HR image, one of the solutions is to develop more advanced optical devices. As the spatial resolution is governed by the CCD array and optical lens, reducing the pixel size is one of the most direct approaches to increase the spatial resolution. However, as the pixel size decreases, the amount of available light also decreases, and the image quality becomes severely degraded by shot noise. Furthermore, nonrectangular pixel layouts, as in the hexagonal Fujifilm super CCD and the orthogonal-transfer CCD [18, 19], have been used to increase the spatial sampling rate, as shown in Fig. 2. Other approaches include increasing the focal length or the chip size. However, a longer focal length will lead to an increase in the size and weight of cameras, while a larger

chip size will result in an increase in capacitance. Therefore, both of these approaches are not considered to be effective due to the limitations of the sensors and the optics manufacturing technology [4]. Compared with CMOSs, CCDs have advantages in sensor sensitivity, imaging resolution, noise suppression and technology maturity [20]. However, considering the high cost of current CCD-based cameras, CMOS-based technologies have recently been investigated. For example, Scientific CMOS (sCMOS) sensors feature a higher resolution and high signal-to-noise ratio (SNR); however, the practical use of this technology remains a problem [21]. Overall, due to the limitations of hardware technology, it is still necessary to study SR algorithms to achieve the goal of resolution enhancement.

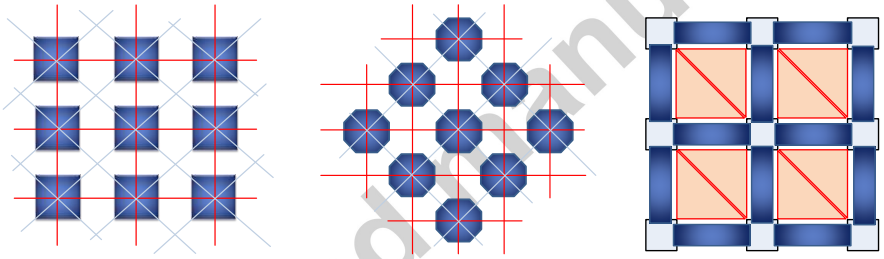

(a) (b) (c)

Fig. 2. The basic CCD types [18]: (a) conventional CCD, (b) super CCD with a nonrectangular pixel layout, and (c) orthogonal-transfer CCD.

Based on the concept of SR, the first problem we need to discuss is the conditions to obtain an HR image from multiple LR observed images. In general, if there is supplementary information among the images, SR is feasible [22]. That is to say, the LR observations cannot be obtained from each other by a transformation or resampling process, thus they contain different information which can be used for SR. If the relative shifts between the LR images are integral, the images after motion

registration will contain almost the same information. As a result, SR cannot obtain effective results.

To implement SR in a real application, researchers have attempted to acquire the images for SR through hardware control. By means of designing the imaging mechanism by hardware techniques, the sensors can acquire observations with known sub-pixel displacements, or multiple "looks" for the same scene. SR is therefore possible. Successful examples can be found in various fields [2, 23-26]. One of the most famous successful cases is in the field of remote sensing. In the French space agency's SPOT-5 satellite system, a specially developed CCD detector was used which packages two 12000-pixel CCDs in one structure. Two line-array CCDs are shifted with each other by half a pixel width in the line-array direction, as shown in Fig. 3 [23]. Since the two CCD detectors can capture images at the same time, a set of data can therefore be acquired at a half-pixel shift in the imaging position. Using this device and SR techniques, we can obtain a HR image from the two sub-pixel shifted images. Leica ADS40 aerial cameras have adopted a similar imaging mechanism to SPOT-5 [27, 28]. Moreover, some CCD pixels comprise sub-pixels with different shapes and spatial locations [29]. By combining multiple images recorded with different sub-pixel components, we can obtain a higher-resolution image via SR.

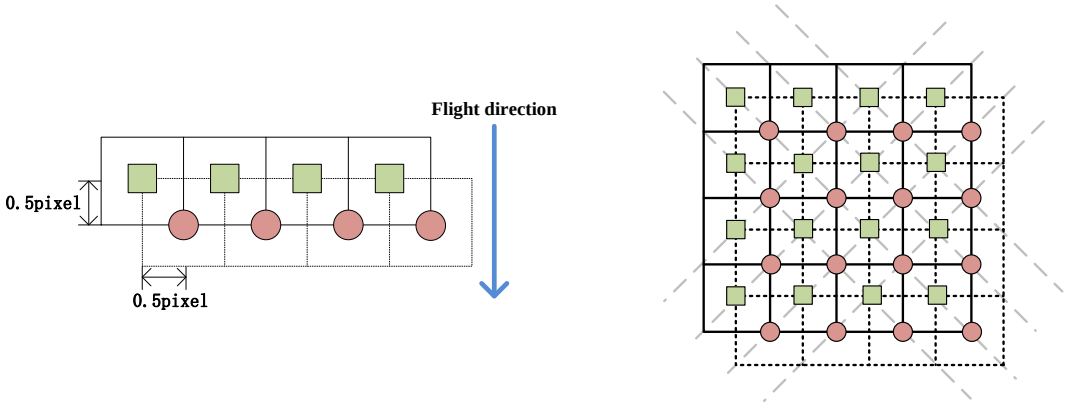

(a) (b)

Fig. 3. Sub-pixel imaging for SPOT-5 [23]. A double CCD linear array in (a) generates two classical square sampling grids in (b), shifted by half a sampling interval in both row and column directions.

3. Super-resolution technologies and methods

In this part, we discuss the methods and current problems for SR with multiple observations. The key problem is how to use the supplementary information among the acquired repeat-pass images. In 1964, Harris [30] established the theoretical foundation for the SR problem by introducing the theorems of how to solve the diffraction problem in an optical system. Two decades later, Tsai and Huang [31] first addressed the idea of SR to improve the spatial resolution of Landsat TM images. Since then, many researchers have begun to focus on SR, either in theoretical research or practical applications [1, 2, 22, 24-26, 28, 32-70]. SR has now been developed for more than three decades, and the progress of SR can be roughly summarized as follows.

At the very start, most of the methods concentrated on the frequency domain [31, 33, 59-61]. Frequency domain algorithms can make use of the relationship between the HR image and the LR observations based on a simple theoretical basis, and have high

computational efficiency. However, the methods have apparent limitations, such as sensitivity to model errors and difficulty in handling more complicated motion models, which have prevented them from further development.

Due to the drawbacks of the frequency domain algorithms, spatial domain methods then became the main trend [4]. The popular spatial domain methods include non-uniform interpolation [35], iterative back-projection (IBP) [56], projection onto convex sets (POCS) [57, 63, 70], the regularized methods [34, 40, 43, 47, 53, 54, 58, 62], and a number of hybrid algorithms [71]. Early review papers have provided specific descriptions and explanations of those methods [4, 8, 14]. Among them, the regularized methods are the most popular due to their effectiveness and flexibility. Therefore, most of the recent representative articles about SR have focused on regularized frameworks [1, 47, 49, 53, 54, 68, 72, 73]. In this part, our emphasis is to review the development of the regularized methods, especially over the last decade. Furthermore, the related research progress into parameter setup and optimization algorithms is also summarized. The remainder of this part is structured as follows. Firstly, we talk about the imaging models. The related models are then described, including the data fidelity and regularization terms. Some advanced techniques and challenges are then discussed, including adaptive parameter setup, blind reconstruction, and optimization strategies.

3.1 The observation model

The imaging model, which refers to the observation model, is essential to SR when

using a regularized framework. Before reconstruction, we need to clarify the process by which the observed images have been obtained. The image acquisition process is inevitably confronted with a set of degrading factors, such as optical diffraction, under-sampling, relative motion, and system noise. In general, we usually suppose that the degradation procedure during image acquisition involves warping, blurring, down-sampling, and noise (Fig. 4), and the observation model is simulated as follows:

$$\boldsymbol{y}_k = \boldsymbol{O}_k \boldsymbol{D}_k \boldsymbol{B}_k \boldsymbol{M}_k \boldsymbol{z} + \boldsymbol{n}_k \quad (1)$$

where there are K LR images participating in the reconstruction. As $N_{1k} \times N_{2k}$ is defined as the size of the kth input LR image, $L_{1k}N_{1k} \times L_{2k}N_{2k}$ is set as the size of the reconstructed HR data, which is determined by the horizontal and vertical magnification factors L_{1k} and L_{2k}. In (1), $\boldsymbol{z}$ is the vector form of the reconstructed image with a size of $L_{1k}N_{1k}L_{2k}N_{2k} \times 1$, which is given as $\boldsymbol{z} = \left[z_1, z_2, \cdots, z_{L_{1k}N_{1k}L_{2k}N_{2k}} \right]^T$, and $\boldsymbol{y}_k = \left[y_{k,1}, y_{k,2}, \cdots, y_{k,N_{1k}N_{2k}} \right]^T$ is the vector form of the kth input dataset. $\boldsymbol{D}_k$ is the down-sampling matrix of size $N_{1k}N_{2k} \times L_{1k}N_{1k}L_{2k}N_{2k}$, $\boldsymbol{B}_k$ represents the blurring operator with size of $L_{1k}N_{1k}L_{2k}N_{2k} \times L_{1k}N_{1k}L_{2k}N_{2k}$, and $\boldsymbol{M}_k$ is the warp matrix describing the motion information (e.g. translation, rotation, etc.). $\boldsymbol{n}_k$ ($N_{1k}N_{2k} \times 1$) indicates the additive noise. $\boldsymbol{O}_k$ is the operator excluding the unobservable pixels from the kth image [47, 74, 75]. In this way, we can deal with the inpainting and SR problem simultaneously if there are invalid pixels and/or motion outliers in the LR images (Fig. 4).

We can obtain the observation model for single-frame SR when $K = 1$ in (1). If $\boldsymbol{D}_k$ and $\boldsymbol{M}_k$ are excluded, it is a model for image restoration, only dealing with the

problems of noise, blurring, or missing information. For convenience of expression, we rewrite model (1) by substituting the product of $\boldsymbol{O}_k$, $\boldsymbol{D}_k$, $\boldsymbol{B}_k$, and $\boldsymbol{M}_k$ by $\boldsymbol{H}_k$, which is as follows:

$$\boldsymbol{y}_k = \boldsymbol{H}_k \boldsymbol{z} + \boldsymbol{n}_k \tag{2}$$

The model in (1) is still insufficient for expressing all possible situations. As a result, other models take more complicated factors into consideration to better describe real cases, including different kinds of noise [52, 76], dimensional complexity [51], domain transformation for the particular images [77], etc. These models are not discussed in detail in this paper.

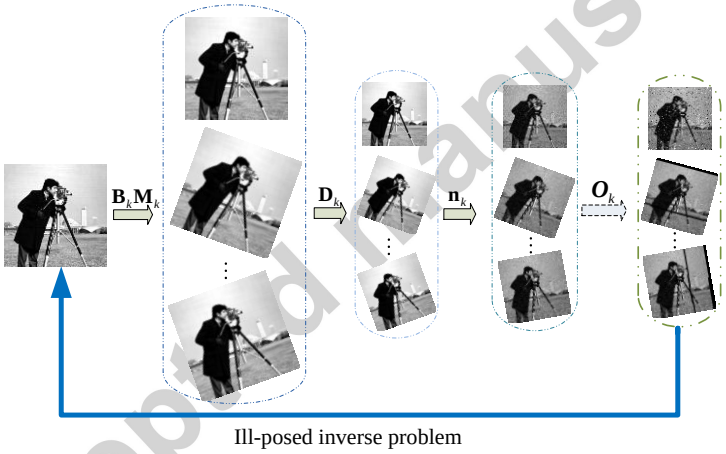

Fig. 4. The super-resolution imaging model. $\boldsymbol{B}_k$, $\boldsymbol{M}_k$ and $\boldsymbol{D}_k$ indicate the blur matrix, warp matrix and down-sampling matrix, respectively. $\boldsymbol{n}_k$ represents the additive noise, while $\boldsymbol{O}_k$ is the operator cropping the observable pixels from $\boldsymbol{y}_k$.

3.2 Regularized reconstruction methods

3.2.1. The regularized framework

Based on the observation model described above, the target is to reconstruct the HR

image from a set of warped, blurred, noisy, and under-sampled measured images. As the model in (2) is ill-conditioned, SR turns out to be an ill-posed inverse problem. Based on maximum a posteriori (MAP) theory, the problem we need to solve can be transformed to the minimization problem as [62, 78]:

$$E(\boldsymbol{z}) = \arg\min_{\boldsymbol{z}} \sum_{k=1}^{K} \rho\left(\boldsymbol{y}_k - \boldsymbol{H}_k \boldsymbol{z}\right) + \lambda U\left(\boldsymbol{z}\right) \tag{3}$$

where $\rho(\cdot)$ and $U(\cdot)$ indicate the corresponding constraint functions. In (3), the first term is the data fidelity term, and the second term is the regularization term, with $U(\boldsymbol{z})$ being the energy function. λ is the regularization parameter balancing these two terms. This is the general variational regularized SR framework. Without the regularization term, this is equal to maximum likelihood (ML) estimation. The MAP methods incorporate the prior constraints of the image, and obtained the results by maximizing the cost function of the posterior probability. They are popular for their flexibility with edge-preserving priors and joint parameter estimation. Comparatively, Bayesian estimation are used when the posteriori probability distribution of the unknown parameters, instead of the specific parameters, is estimated.

3.2.2. The data fidelity term

The data fidelity term is used to constrain the residuals between the real LR images and the simulated ones obtained, and it is usually associated with the noise model. For instance, the l_2 norm based linear least-squares term is widely used [41, 49, 62, 79, 80], as $p = 2$ in (4). The main advantage of the l_2 norm problem is that it is easy to solve, and many efficient algorithms exist [43, 81]. However, the result solved by the

l_2 model is only optimal when the model error is white-Gaussian distributed [82].

$$F(\boldsymbol{z}) = \sum_{k=1}^{K} \left\| \boldsymbol{y}_k - \boldsymbol{H}_k \boldsymbol{z} \right\|_p^p \tag{4}$$

As a result, there has been a growing interest in choosing the l_1 norm as the function $\rho(\cdot)$ in (4) for image SR and restoration, where $p=1$ in (4). As the l_2 norm corresponds to Gaussian distributed errors, the l_1 norm mainly corresponds to the Laplacian error model, as shown in Fig. 5. According to Farsiu et al. [43], $p=1$ results in a pixel-wise median and $p=2$ leads to a pixel-wise mean of all the measurements after motion compensation in the SR model. It has been proven that the l_1-norm fidelity is more effective than the l_2-norm fidelity when the images contain non-Gaussian errors [43, 83].

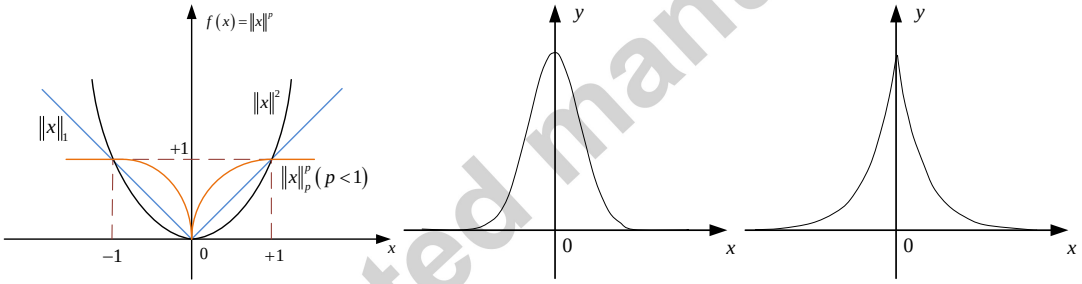

(a) (b) (c)

Fig. 5. The properties of different norm functions and the error distribution, where (b) and (c) indicate the distribution for Gaussian and Laplacian errors, respectively. The l_2 norm corresponds the quadratic curve in (a), which is consistent with the Gaussian distribution in (b). In contrast, the plot of l_1 norm is more consistent to the Laplacian distribution.

For complicated types of noise and/or model error, however, both the l_1 norm and the l_2 norm have their advantages and disadvantages. Some researchers have therefore employed improved techniques for the data fidelity term [52, 81, 84-87]. In cases with mixed error modes, the l_p norm function ($1 \le p \le 2$) is sometimes

employed as the constraint function because of its convex property and its pertinence for the imaging model errors [81]. When $1 \le p \le 2$, it results in a weighted mean of measurements. If the value of p is close to one, then the solution is calculated with a larger weight around the measurements near the median value. When the value of p is near to two, the solution is approximated to the average value [43]. In some cases, images are contaminated by both Gaussian and non-Gaussian errors, and the l_p norm function is considered to be an effective solution [81, 82]. According to the imaging model, detecting the outliers and restoring them in matrix $\boldsymbol{O}_k$ as unobservable pixels is also an effective way to exclude the impulse noisy pixels and the motion outliers belonging to non-Gaussian errors [47].

The comparative reconstruction results for the different fidelity norms are given in Figs. 6–7. In the first case, the synthetic test was conducted with the Lena test image, in which the original image was first down-sampled by a factor of two in both the horizontal and vertical directions. Thus, four LR images were obtained, with the translational shifts being (0, 0), (0, 0.5), (0.5, 0), and (0.5, 0.5). A mixed mode of Gaussian (normalized variance 0.003) and impulse noise (density 0.03) was then added in the LR images. In the Foreman experiment, five degraded images with moving objects were included in the reconstruction, and the 24th frame of the video sequence was set as the reference frame. The LR images were obtained using the corresponding HR frames in the video, with a down-sampling factor of two. We evaluate the results of the synthetic experiments using the peak signal-to-noise ratio (PSNR) and the structural similarity (SSIM) index [88]. The PSNR is used to evaluate

the gray value similarity, while the SSIM is mainly employed to reflect the structural similarity [89].When images are contaminated with mixed noise (Fig. 6), the l_2 norm cannot completely remove the speckles while preserving the texture. In contrast, the l_1 norm has some problems in dealing with Gaussian-distributed noise, and the l_p norm can obtain better results, in terms of both the visual effect and quantitative indexes. In the second test, it can be clearly seen that l_1 and l_p are more robust than l_2 when dealing with motion outliers in the LR observations. With the ability to deal with motion outliers, both l_1 and l_p can prevent the reconstructed details from being oversmooth. Furthermore, the $l_p - norm$ fidelity can achieve a balance between removing noise and suppressing motion artifacts in the noisy cases [52].

PSNR: 22.026 SSIM: 0.530 (a)

PSNR: 26.108 SSIM: 0.730 (b)

PSNR: 28.040 SSIM: 0.787 (c)

PSNR: 28.311 SSIM: 0.801 (d)

Fig. 6. The SR reconstruction results of the Lena image by (a) bilinear interpolation, and (b) MAP with l_2-norm fidelity, (c) l_1-norm fidelity, and (e) l_p-norm fidelity, with p=1.3.

PSNR: 32.671 SSIM: 0.921

PSNR: 35.683 SSIM: 0.942

PSNR: 36.542 SSIM: 0.960

PSNR: 36.675 SSIM: 0.959

Fig. 7. The SR reconstruction results of the noiseless Foreman image by (a) bilinear interpolation, and (b) MAP with l_2-norm fidelity, (c) l_1-norm fidelity, and (e) l_p-norm fidelity, with p=1.5.

A weighted data fidelity term is also suitable for some cases in which the LR images make different contributions to the reconstructed image [25, 79, 90]. In some practical cases, the amount of available information contained in each LR image might differ according to the image quality (e.g., noise level, spatial resolution, angle, etc.). Thus, different weights should be considered in such cases, as in (5). A weighted data fidelity term has been widely used in the related works, and different methods were presented to determine w_k [25, 79, 90]. The core idea is to discriminate between the different contributions of the LR images involved in SR.

$$F(\boldsymbol{z}) = \sum_{k=1}^{K} w_k \cdot \left\| \boldsymbol{y}_k - \boldsymbol{H}_k \boldsymbol{z} \right\|_p^p \tag{5}$$

3.2.3. The regularization term

The regularization plays a significant role in the regularized variational framework. As SR is a classical ill-posed inverse problem, regularization is therefore adopted to stabilize the inversion process [4, 47, 91]. According to the Bayesian theorem, the regularization term represents the image prior modeling, providing the prior knowledge about the desired image [4, 72, 92]. Over the past 10 years of vigorous development, there have been a large amount of studies of regularization for image restoration and SR [81, 89, 93-98].

- **Smoothness prior models**

In the early years, the smoothness of natural images was mainly considered, which leads to the quadratic property of the regularizations [99, 100]. Tikhonov-based regularization is the representative smoothing constraint, whose energy function is

usually defined as:

$$U(\boldsymbol{z}) = \|\boldsymbol{\Gamma z}\|_2^2 \tag{6}$$

where $\boldsymbol{\Gamma}$ is usually chosen as an identity matrix or high-pass operator (e.g., a difference operator or a weighted Fourier operator). Laplacian regularization is one of the most common regularizations used in SR, and was developed from Tikhonov regularization by choosing the smoothing operator as the discrete 2-D operator [100].

Another category of regularization is based on Markov theory. A Markov random field (MRF) assumes that the value of a pixel is only related to the adjacent pixels, which satisfy a Gibbs density function [50]. In this way, MRF can efficiently describe the local statistical characteristics of images. The energy function can be given as:

$$U(\boldsymbol{z}) = \sum_{c \in C} V_c(\boldsymbol{z}) = \sum_{t=1}^{\tau} \phi\left(d_c^t \boldsymbol{z}\right) \tag{7}$$

where d_c^t is a coefficient vector for clique c, which is usually defined as the finite-difference approximations to second-order derivatives in the four directions. $\phi(\cdot)$ is the constraint function. The regularization function is usually divided into two categories, Gaussian MRF (GMRF) [78] or Huber MRF (HMRF) [101], in accordance with the choice of $\phi(\cdot)$. For GMRF regularization, the quadratic l_2 norm is employed for $\phi(\cdot)$.

These regularized methods smooth the restored image by penalizing the high-frequency component, and thus perform well in suppressing noise. However, they inevitably oversmooth the sharp edges and detailed information.

◆ **Edge-preserving prior models**

The smoothing prior models are somewhat against the nature of images, in that

sharp details in images are always desirable for human beings in many applications, including remote sensing imaging, medical diagnosis and object recognition [2, 28, 69]. Thus, $l_1 - norm$ based regularizations are often preferred for their edge-preserving properties [93, 101, 102]. The representative total variation (TV) regularization was first proposed by Osher et al. [93, 103], based on the fact that an image is naturally "blocky" and discontinuous. The standard TV norm is given as:

$$U(\boldsymbol{z}) = \sqrt{(\nabla^x \boldsymbol{z})^2 + (\nabla^y \boldsymbol{z})^2 + \beta} \tag{8}$$

where $\nabla^x \boldsymbol{z}$ and $\nabla^y \boldsymbol{z}$ are the first-order image gradients in the horizontal and vertical directions, respectively. Here, β is a small scalar to ensure differentiability.

Unlike the quadratic regularizations, edge information can be better preserved using TV regularization, with the l_1 norm to deal with the image information rather than the l_2 norm [47, 104, 105]. Therefore, the TV prior model has been the most popular model for image processing in the last two decades, and has been applied in fields such as image denoising, deblurring, segmentation, and SR [47, 76, 104, 106]. However, the results of the TV prior model will often result in a "staircase" effect with strong noises, especially in flat regions [89].

To overcome the shortcomings of the TV prior model, some researchers have proposed spatially adaptive strategies. A number of methods use spatially adaptive regularization parameters to eliminate the staircase effects [94, 107-109]. Some of them classified the image into detailed and flat regions using the spatial information, and used a larger penalty parameter for the flat regions and a smaller one for the edges [94, 107]. However, the spatially adaptive indicators such as gradients, the difference

curvature, and structure tensor are usually sensitive to noise.

Moreover, different norm constraints can also be employed for the prior modeling in a spatially adaptive way [96, 108]. The l_p norm, rather than the l_1 norm, can be used as the constraint function for $\nabla \boldsymbol{z}$ in the TV term. As the l_2 norm represents a smoothing prior and the l_1 norm tends to preserve the edges, the l_p $(1 \le p \le 2)$ norm achieves a balance between them, thereby avoiding the staircase effect [110]. Other improvements include higher-order TV (HDTV) [111], bilateral TV (BTV) [43], locally adaptive BTV (LABTV) [96], etc.

HMRF is also a representative edge-preserving prior model [101, 112]. A hybrid norm can theoretically achieve a balance between preserving edges and suppressing noise, to some degree. For the HMRF term, $\phi(\cdot)$ in (7) is chosen as the Huber function, which is piecewise as:

$$\phi(x) = \begin{cases} x^2 & x \le T \\ 2T|x| - T^2 & x > T \end{cases} \tag{9}$$

where T is the threshold. The Huber function satisfies the properties of convexity, symmetry, and discontinuity. The HMRF model is effective when dealing with images with clear texture. However, only the neighborhood information is considered, which limited its performance [113].

◆ **Nonlocal-based priors**

The local derivatives are somewhat sensitive to noise in the images' homogenous regions, which negatively affects the reconstruction effect in noisy cases. Recently, the concept of nonlocal-based priors has been proposed and has developed rapidly in image processing [97, 114-116]. Rather than defining the neighborhood of a pixel

locally, nonlocal-based priors consider pixels in a large search area and weight them according to the similarity between rectangular patches. This is based on the assumption that every feature in a natural image can be found many times in the same scene [114]. The nonlocal models have become popular in the regularized framework, given the nonlocal TV regularization as:

$$U_{NLTV}(\boldsymbol{z}) = \sum_{x \in \boldsymbol{\Omega}} \sum_{y \in \Pi_x} w(x,y) \left| \boldsymbol{z}(x) - \boldsymbol{z}(y) \right| \qquad (10)$$

where x indicates one of the pixels in the image $\boldsymbol{z}: \Omega \to \mathbb{R}$, and the search window is usually restricted to the square neighborhood of x, denoted as Π_x. The weight function $w(x,y)$ can then be defined as:

$$w(x,y) = \exp\left(-\frac{\left\| P_x(\boldsymbol{z}) - P_y(\boldsymbol{z}) \right\|_p^p}{\sigma^2} \right) \qquad (11)$$

Here, $P_x(\boldsymbol{z})$ and $P_y(\boldsymbol{z})$ represent the $(2n+1)\times(2n+1)$ patch of $\boldsymbol{z}$, centered at the pixel x (or y) with a radius of n. The similarity can be calculated with various distance formulas (e.g., by choosing different values of p). σ is the filtering parameter. Compared with the TV model, the nonlocal-based model can make use of more information, and can thus prevent the staircase effect in flat regions, and can help restore the details [97, 113].

The comparative results of the typical regularizations are displayed in Fig. 8. The down-sampling process was set the same as for the Lena image in Section 3.2.2. The generated LR images were then blurred by a 3*3 filter with a variance of 1, and contaminated by Gaussian noise with a standard variance of 10. From the results, it

can be seen that all the edge-preserving regularizations perform well in removing noise and preserving the details. Nevertheless, the results of the HMRF and nonlocal TV models better conform to human visual perception.

Fig. 8. The SR reconstruction results using different regularizations. Top row: bilinear interpolation, Laplacian regularization, and HMRF regularization [100]. Bottom row: TV regularization [47], NLTV regularization [114], and the original HR image.

In addition to the above regularizations, there have been many other studies of prior models, such as regularization based on sparsity [117], along with morphological theory [98]. The common goal of all these methods is that they want to reconstruct a noiseless HR image with natural texture and clear, detailed information. There have also been studies of spectral images (e.g., digital color images or hyperspectral images), where the emphasis has been on the preservation of spectral information, while enhancing the spatial resolution [118, 119].

3.2.4. Adaptive regularization parameter selection

Parameter selection is always a headache when dealing with ill-posed inverse problems. The regularization parameter, in particular, plays a significant role in image SR. In this part, we present the main approaches to adaptive strategies for determining the regularization parameter λ in (6).

In many cases, the regularization parameter is selected manually. The common approach is to test a sequence of regularization parameters and select the optimal parameter corresponding to the best results evaluated by quantitative indexes or visual inspection. This is, however, a time-consuming and subjective process. Therefore, adaptive strategies are necessary in the SR process. A number of strategies have been specially designed to adaptively estimate the regularization parameter. These strategies have mainly been inspired by developments in the inverse problem field, such as denoising and deblurring [120-123]. The popular methods include the L-curve method [124], generalized cross-validation (GCV) [35], and the U-curve method [49].

It has been noted in the earlier studies that the GCV method tends to give unsatisfactory results if the model errors are highly correlated [121]. The L-curve method has some advantages over GCV, including well-defined numerical properties and robustness in dealing with highly correlated errors. Both of the L-curve and U-curve methods are based on the parametric plots generated by varying the regularization parameter λ. The target is to find the optimal λ that achieves a good balance between minimizing the data fidelity and regularization. As the $l_2 - norm$ based model is chosen, the energy function can be given as:

$$E(\boldsymbol{z}) = \arg\min_{\boldsymbol{z}} \sum_{k=1}^{K} \left\| \boldsymbol{y}_k - \boldsymbol{H}_k \boldsymbol{z} \right\|^2 + \lambda \left\| \boldsymbol{\Gamma} \boldsymbol{z} \right\|^2 \tag{12}$$

where $\boldsymbol{\Gamma}$ indicates the two-dimensional Laplacian operator. After using the singular value decomposition (SVD) least-squares method for $\boldsymbol{H}_k$, we define:

$$R(\lambda) = \sum_{k=1}^{K} \left\| \boldsymbol{y}_k - \boldsymbol{H}_k \hat{\boldsymbol{z}}_\lambda \right\|^2, P(\lambda) = \left\| \boldsymbol{\Gamma} \hat{\boldsymbol{z}}_\lambda \right\|^2 \tag{13}$$

The L-curve method searches for the distinct L-shaped corner using the relationship between $R(\lambda)$ and $P(\lambda)$, while the U-curve method selects the maximum curvature point close to the left vertical part of the U-curve ($U(\lambda) = \frac{1}{R(\lambda)} + \frac{1}{P(\lambda)}$) as the optimal parameter. It has been proved that the U-curve method can obtain more accurate solutions in quadratic cases for SR. Further details can be found in the related works [49, 124]. These methods can obtain relatively good solutions, but they have not yet been extended to the general regularized framework with various regularizations.

It has to be mentioned that the Bayesian framework [53, 72] is also a powerful tool for modeling unknown parameters, including the regularization parameter, the blur kernel, and motion vectors. We discuss the Bayesian methods in the next section.

3.2.5. Blind reconstruction

Earlier in this article, we have discussed the main developments in the SR framework based on MAP theory, from the point of view of data fidelity and regularization. However, the techniques mentioned before are used with the assumption that the parameters, such as the motion model, blur kernel, and noise level,

are known [62]. This is impractical in real-world cases, where the motion of objects and cameras cannot be estimated beforehand. In addition, the point spread functions (PSFs) and the noise level are always unknown.

The traditional methods deal with parameter estimation and reconstruction separately. These methods regard registration and blur kernel identification as a preprocessing stage [43, 79, 96]. However, the parameters estimated using only the LR images can be inaccurate, which will lead to an unsatisfactory performance. We introduce two effective strategies for blind reconstruction below.

◆ **The joint MAP framework**

The MAP framework is advantageous in parameter estimation due to its flexibility in adding priors for the unknown parameters [4]. Therefore, some researchers have developed joint MAP methods to adaptively obtain the unknown parameters [62, 125, 126]. Similar to the observation model in (1), we define the LR observations as $\boldsymbol{y}=\left[\boldsymbol{y}_1^T,\boldsymbol{y}_2^T,\cdots,\boldsymbol{y}_K^T\right]^T$, the motion vectors as $\boldsymbol{s}=\left[\boldsymbol{s}_1^T,\boldsymbol{s}_2^T,\cdots,\boldsymbol{s}_K^T\right]^T$, and the PSFs as $\boldsymbol{h}=\left[\boldsymbol{h}_1^T,\boldsymbol{h}_2^T,\cdots,\boldsymbol{h}_K^T\right]$. The observation model in (1) can then be expressed in matrix notation as (14):

$$\boldsymbol{y}=\boldsymbol{ODB}\left(\boldsymbol{h}\right)\boldsymbol{M}\left(\boldsymbol{s}\right)\boldsymbol{z}+\boldsymbol{n} \tag{14}$$

Noting that $\boldsymbol{z}$, $\boldsymbol{h}$, and $\boldsymbol{s}$ are statistically independent, we can form an estimate of the unknown parameters simultaneously, according to the theory of MAP. Once we determine the probability density function (PDF) of $\boldsymbol{z}$, $\boldsymbol{h}$, and $\boldsymbol{s}$, the ill-posed inverse problem can be solved by optimizing the following cost function:

$$\hat{\boldsymbol{z}},\hat{\boldsymbol{h}},\hat{\boldsymbol{s}}=\arg\min_{\boldsymbol{z},\boldsymbol{h},\boldsymbol{s}}\left\{\left\|\boldsymbol{y}-\boldsymbol{ODB}\left(\boldsymbol{h}\right)\boldsymbol{M}\left(\boldsymbol{s}\right)\boldsymbol{z}\right\|_p^p+\lambda_1 U\left(\boldsymbol{z}\right)+\lambda_2 U\left(\boldsymbol{h}\right)+\lambda_3 U\left(\boldsymbol{s}\right)\right\} \tag{15}$$

The estimated parameters are iteratively updated along with the reconstructed image in a cyclic optimization procedure. However, there will be a number of unknown parameters which need to be tuned.

◆ **The Bayesian framework**

Differing from the MAP estimator, the Bayesian methods calculate the posterior distribution instead of setting specific values of the parameters for the SR system [72, 127]. Both the ML and MAP estimators return only single and specific values for the parameters, while Bayesian estimation, in contrast, fully calculates the posterior distribution $p(\boldsymbol{z},\boldsymbol{h},\boldsymbol{s}|\boldsymbol{y})$.

The Bayesian inference is based on the posterior distribution, and thus:

$$p(\boldsymbol{z},\boldsymbol{h},\boldsymbol{s}|\boldsymbol{y}) = \frac{p(\boldsymbol{z},\boldsymbol{h},\boldsymbol{s},\boldsymbol{y})}{p(\boldsymbol{y})} \tag{16}$$

Here $p(\boldsymbol{z},\boldsymbol{h},\boldsymbol{s},\boldsymbol{y})$ refers to $p(\boldsymbol{y}|\boldsymbol{z},\boldsymbol{h},\boldsymbol{s})\,p(\boldsymbol{z})\,p(\boldsymbol{h})\,p(\boldsymbol{s})$ for the convenience of expression. $p(\boldsymbol{y})$ is independent of the unknown variables, and is usually ignored in the MAP estimator. In fact, as in many applications, $p(\boldsymbol{z},\boldsymbol{h},\boldsymbol{s}|\boldsymbol{y})$ is intractable because $p(\boldsymbol{y})$ cannot be computed [72]. Approximation methods need to be utilized for the reconstruction [45, 53, 72]. In Babacan's work [72], they utilized a variational Bayesian method by minimizing the Kullback-Leibler (KL) distance between the posterior $p(\boldsymbol{z},\boldsymbol{h},\boldsymbol{s}|\boldsymbol{y})$ and a tractable distribution $q(\boldsymbol{z},\boldsymbol{h},\boldsymbol{s})$. Assuming the approximated distribution $q(\boldsymbol{z},\boldsymbol{h},\boldsymbol{s})$ can be factorized, the distribution of the corresponding parameter can be estimated by calculating the corresponding expectation using the first-order Taylor series.

By estimating the full posterior distribution of the unknowns instead of point

estimations corresponding to the maximum probability (e.g., MAP), the uncertainty of the estimates is incorporated into the estimation procedure. In addition, the unknown parameters can be estimated during the iterative estimation process [41, 53, 72]. Nevertheless, the accuracy of the Bayesian framework depends on the parameter distribution models, and is influenced by some attached parameters via the iterations.

3.2.6 Optimization methods

After the reconstruction model is built, the HR image can be acquired by optimizing the corresponding cost function. If a Gaussian distribution is chosen for the noise model, and a quadratic constraint is employed for the regularization, then the energy function can be given as (12). The Euler-Lagrange function can be acquired as follows:

$$\nabla E(\boldsymbol{z}) = -\sum_{k=1}^{K} \boldsymbol{H}_k^T \left(\boldsymbol{y}_k - \boldsymbol{H}_k \boldsymbol{z} \right) + \lambda \boldsymbol{\Gamma}^T \boldsymbol{\Gamma} \boldsymbol{z} = 0 \qquad (17)$$

For the quadratic equation, $\boldsymbol{z}^{n+1}$ can be obtained as the solution to the linear equation:

$$\left[\sum_{k=1}^{K} \boldsymbol{H}_k^T \boldsymbol{H}_k - \boldsymbol{\Gamma}^T \boldsymbol{\Gamma} \right] \boldsymbol{z}^{n+1} = \sum_{k=1}^{K} \boldsymbol{H}_k^T \boldsymbol{y}_k \qquad (18)$$

The minimization of the standard $l_2 - norm$ based model is the regularized solution of a linear partial differential equation (PDE). To solve this quadratic ill-posed inverse problem, a conjugate gradient (CG) or preconditioned CG (PCG) method is usually employed to optimize the Lagrangian functional [47, 128]. With the initial estimation

and stopping criterion for the iteration given, the estimated result will approximate the numerical solution via iterations.

However, the l_2 norm-based model cannot acquire satisfactory results in many real cases. Compared with the l_2 norm, it is difficult to employ conventional numerical methods for l_1-norm problems directly, due to the nonlinearity of the l_1 norm function. Moreover, the convergence rate cannot meet the demand of large-scale inverse problems. Some efficient approximation methods have been developed for optimizing the l_1 norm regularized functional [102, 104, 105, 128-131]. Typically, the popular numerical algorithms for the nonlinear SR problems can be roughly classified into two categories, which are: 1) Euler-Lagrange smooth approximation; and 2) primal-dual/splitting algorithms.

◆ **Euler-Lagrange smooth approximation**

As we know, perfect or exact solutions are often difficult to acquire. The common goal is to find the optimal solution in a statistical sense. Euler-Lagrange smooth approximation methods generally use a smooth approximation of the l_1-norm, thus construct a linear functional to optimize. The representative algorithms include lagged diffusivity fixed point iteration (LDFPI) [128], majorization-minimization (MM) [104], the iteratively reweighted norm (IRN) [129, 132], and the half-quadratic algorithm [95]. As one of the most popular regularizations employed in image restoration, the TV model is a classical non-quadratic optimization problem. Here, we take the l_2-TV SR model as an example to show the specific approximation process. The notations are based on LDFPI [128] and IRN [129], respectively. The

reconstruction model can be given as:

$$\hat{\boldsymbol{z}} = \arg\min_{\boldsymbol{z}} \left\{ \sum_{k}^{K} \left\| \boldsymbol{y}_k - \boldsymbol{H}_k \boldsymbol{z} \right\|_2^2 + \lambda \left\| \nabla \boldsymbol{z} \right\|_{TV} \right\} \tag{19}$$

where $\left\| \nabla \boldsymbol{z} \right\|_{TV}$ indicates the isotropic TV regularization defined in (8). The Euler-Lagrange equation for the energy function in (19) is given by the following nonlinear system:

$$\nabla E(\boldsymbol{z}) = \sum_{k} \boldsymbol{H}_k^T \left(\boldsymbol{H}_k \boldsymbol{z} - \boldsymbol{y}_k \right) - \lambda \boldsymbol{L}_{\boldsymbol{z}} \boldsymbol{z} = 0 \tag{20}$$

where $\boldsymbol{L}_{\boldsymbol{z}} = \nabla \cdot \left(\nabla / \sqrt{\left| \nabla \boldsymbol{z} \right|^2 + \beta} \right)$, which is the matrix form of a central difference approximation of the differential operator, with $\nabla \cdot$ being the divergence operator. This is a nonlinear equation for $\boldsymbol{z}$. To transform the functional to a linear PDE, smooth approximation strategies need to be adopted. LDFPI, which was first introduced by Vogel [128], linearizes the differential term by lagging the diffusion coefficient $1/\sqrt{\left| \nabla \boldsymbol{z} \right|^2 + \beta}$ one iteration behind. Thus $\boldsymbol{z}^{n+1}$ is obtained as the solution to the approximated linear equation:

$$\left[\sum_{k} \boldsymbol{H}_k^T \boldsymbol{H}_k - \lambda \boldsymbol{L}_{\boldsymbol{z}}^n \right] \boldsymbol{z}^{n+1} = \sum_{k} \boldsymbol{H}_k^T \boldsymbol{y}_k \tag{21}$$

Usually, half-point discretization [133] is used to approximate $\boldsymbol{L}_{\boldsymbol{z}}^n$. To solve the linear PDE above, a CG or PCG method is desirable. IRN is a method which can minimize the l_p norm ($p \le 2$) by approximating it with a weighted l_2 norm [129].

$$\left\| \boldsymbol{u} \right\|_p^p = \sum_{k} \left(\left| u_k \right|^{p-2} \right) u_k^2 = \sum_{k} w_k {u_k}^2 = \boldsymbol{u}^T \boldsymbol{W} \boldsymbol{u} = \left\| \boldsymbol{W}^{1/2} \boldsymbol{u} \right\|_2^2 \tag{22}$$

where $\boldsymbol{W} = diag\left(\left| \boldsymbol{u} \right|^{p-2} \right)$. Introducing the idea into the energy function in (22), the functional can be expressed as:

$$\boldsymbol{z} = \arg\min_{\boldsymbol{z}} \left\{ \sum_{k}^{K} \left\| \boldsymbol{y}_k - \boldsymbol{H}_k \boldsymbol{z} \right\|_2^2 + \frac{\lambda}{2} \left\| \tilde{\boldsymbol{W}}_R^{1/2} \nabla \boldsymbol{z} \right\|_2^2 \right\} \tag{23}$$

where

$$\tilde{\boldsymbol{W}}_R = \begin{pmatrix} \boldsymbol{W}_R & 0 \\ 0 & \boldsymbol{W}_R \end{pmatrix} \tag{24}$$

Here, we define

$$\boldsymbol{W}_R = diag\left(2 f_R \left(\left(\nabla_x \boldsymbol{z} \right)^2 + \left(\nabla_y \boldsymbol{z} \right)^2 \right) \right) \tag{25}$$

where the constraint function $f_R(x) = \begin{cases} |x|^{-1/2} & if\ |x| > \varepsilon \\ 0 & f\ |x| \le \varepsilon \end{cases}$. Thus, the Euler-Lagrange function can be linearized as:

$$\left[\sum_k \boldsymbol{H}_k^T \boldsymbol{H}_k - \lambda \nabla^T \tilde{\boldsymbol{W}}_R^n \nabla \right] \boldsymbol{z}^{n+1} = \sum_k \boldsymbol{H}_k^T \boldsymbol{y}_k \tag{26}$$

The weight matrix $\tilde{\boldsymbol{W}}_R^n$ can by calculated by (23)–(25) using $\boldsymbol{z}^n$. It appears that LDFPI and IRN are two different methods; however, they are almost the same in essence when dealing with the $l_1 - norm$ problem by smooth approximation. In fact, all the algorithms mentioned above obtain similar results with TV minimization, including LDFPI, IRN, MM, and the half-quadratic algorithm, where lagged iteration was used. Consequently, they can be inferred from each other by transformation. This category of methods is simple to implement, and can be extended to deal with the regularized inversions with various norms.

◆ **Primal-dual/splitting algorithms**

The second group of methods split the original optimization task into a primal

problem and a dual formulation of this problem. In recent years, abundant related studies have been presented, such as the alternating direction method of multipliers (ADMM) [131, 134], the primal-dual (PD) based algorithms [105], the Douglas-Rachford algorithm [135], proximal forward backward splitting (PFBS) [130], and the split-Bregman (SB) method [102]. ADMM is one of the most prevalent methods for convex optimization in image processing. It converts the optimization of the original nonlinear problem into looking for a saddle point of an augmented version of the classical Lagrange function [131]. Given the original model as (19), it can be expressed as the following with an auxiliary variable $\boldsymbol{b}$ introduced:

$$\arg\min_{\boldsymbol{z},\boldsymbol{b}} \left\{ \frac{1}{2} \sum_k \left\| \boldsymbol{y}_k - \boldsymbol{H}_k \boldsymbol{z} \right\|_2^2 + \lambda \left\| \boldsymbol{b} \right\|_1 \right\} \quad s.t. \nabla \boldsymbol{z} = \boldsymbol{b} \tag{27}$$

To transform (27) to generate an unconstrained problem, the augmented Lagrangian can be rewritten as:

$$\mathcal{L}_\tau \left(\boldsymbol{z}, \boldsymbol{b}, \boldsymbol{u} \right) = \left\{ \frac{1}{2} \sum_k \left\| \boldsymbol{y}_k - \boldsymbol{H}_k \boldsymbol{z} \right\|_2^2 + \tau \boldsymbol{u}^T \left(\nabla \boldsymbol{z} - \boldsymbol{b} \right) + \frac{\tau}{2} \left\| \nabla \boldsymbol{z} - \boldsymbol{b} \right\|_2^2 + \lambda \left\| \boldsymbol{b} \right\|_1 \right\} \tag{28}$$

where $\boldsymbol{u}$ is the introduced as Lagrangian multiplier, and $\tau > 0$ is the penalty parameter. It is easy to minimize the objective function in (28) with respect to either $\boldsymbol{z}$ or $\boldsymbol{b}$. The optimization expression can be given by (29):

$$\begin{aligned} \boldsymbol{z}^{n+1} &:= \left(\sum_k \boldsymbol{H}_k^T \boldsymbol{H}_k - \tau \nabla^T \nabla \right)^{-1} \left(\sum_k \boldsymbol{H}_k^T \boldsymbol{y}_k + \tau \nabla^T \left(\boldsymbol{b}^k - \boldsymbol{u}^k \right) \right) \\ \boldsymbol{b}^{n+1} &:= S_{\lambda/\tau} \left(\nabla \boldsymbol{z}^{n+1} + \boldsymbol{u}^n \right) \\ \boldsymbol{u}^{n+1} &:= \boldsymbol{u}^n + \left(\nabla \boldsymbol{z}^{n+1} - \boldsymbol{b}^{n+1} \right) \end{aligned} \tag{29}$$

For a fixed $\boldsymbol{b}$, it turns out to be a quadratic functional for the variable $\boldsymbol{z}$. The generalized shrinkage formula in the second formula is usually employed to solve the

minimization problem for $\boldsymbol{b}^{n+1}$. Finally, the residual term is added to refine the optimization process. Through the alternating iterations, the variables can finally converge to the solution of the original model [131]. The model can be easily extended to more complex models, e.g., a non-quadratic functional with an $l_1 - norm$ data fidelity term.

The relationships between these methods have been discussed in detail in [136]. The Bregman iterative regularization method, the Douglas-Rachford algorithm, and ADMM have been shown to be equivalent under the assumption of linear constraints [136, 137]. The most promising aspect of these methods is that by splitting the original large-scale inverse problem into several sub-problems, the computational efficiency can be greatly improved. In general, the PD-based methods are faster than the optimization algorithms based on smooth approximation.

There are also other fast and robust optimization methods for image SR. For example, graph-cut based methods can be applied for the minimization of graph-based energy functions [138, 139].

3.3 The main challenges for image super-resolution

Although SR techniques have been developed for three decades, there are some pivotal difficulties. In this section, the main challenges for image SR and the corresponding strategies to deal with these issues are discussed. The challenges are: 1) SR with complex motion conditions; 2) SR without multiple LR images; and 3) acceleration strategies for "big data" processing.

3.3.1. Super-resolution with complex motion conditions

It is a big challenge to achieve accurate motion estimation in complex motion conditions. As a result, the performance of the reconstruction-based SR algorithms is significantly affected. Researchers have therefore attempted to deal with the problems brought about by inaccurate motion registration. The solutions include more advanced registration strategies, robust fidelity models, joint parameter estimation, and methods without explicit motion estimation.

- **Advanced registration strategies**

In simulated cases, the sub-pixel motion fields between the reference frame and the other frames can be described by a parameter model (e.g., pure translation or global affine warp). However, they have to be estimated point-wise or block-wise under most practical cases with more complicated motion conditions. Optical flow estimation [140] is one of the representative methods to obtain a relatively accurate motion field of all the points. However, the optical flow based methods are computationally expensive [141] and are sensitive to noise, large displacements, and illumination variation [142]. To increase the accuracy of motion estimation in SR, advanced registration methods are necessary. Baboulaz and Dragotti [143] proposed an advanced method to extract features in LR images for registration by taking a sampling perspective. Su et al. [144] attempted to avoid inaccurate flow estimation by accurately estimating the local flow, based on the sparse feature point correspondences.

- **Robust fidelity models**

Although more accurate registration methods have been applied, motion errors are inevitable in real cases. Researchers have therefore tried to overcome the influence of inaccurate registration from the perspective of model construction. The effects of the registration error are mainly embodied in the data fidelity term, which provides a constraint for the conformance of the reconstructed HR image to the observed LR image. As mentioned in Section 3.2.2, the l_1 norm performs more robustly in dealing with registration errors than the l_2 norm [43]. Thus, $l_1 - norm$ based SR methods can effectively overcome the influence of motion errors. In addition, as expressed in (5), LR images with a large registration error will make less contribution in the reconstruction process by importing the adaptive channel function w_k [145]. The weight w_k is usually set as inversely proportional to $\|\boldsymbol{y}_k - \boldsymbol{H}_k \boldsymbol{z}\|_p^p$ $(1 \le p \le 2)$, and thus reduces the effect of model errors. However, both the $l_1 - norm$ based and weighted models need an extra registration method for motion estimation. Furthermore, the relatively poor convergence performance limits their application.

◆ **Joint parameter estimation**

One of the most popular strategies for improving the reconstruction performance is the joint methods. These approaches (discussed in Section 3.2.5) can obtain better registration results and exclude errors during the iteration by simultaneously estimating the motion parameters and the reconstruction result. Specifically, Tom and Katsaggelos [146] developed a simultaneous registration and reconstruction approach where they formulated the SR problem in the ML framework, and solved it using an

expectation-maximization algorithm. Hardie et al. [100] combined a joint approach and a MAP framework to reconstruct the HR image.

The common assumption is that the blur kernel is known in the reconstruction system. The ill-posed inverse problem can be solved by selecting the appropriate PDF of $\boldsymbol{z}$ and $\boldsymbol{s}$. The choice of prior model $U(\boldsymbol{z})$ and $U(\boldsymbol{s})$ in (15) should accurately describe the characteristics of the realization. However, it is a difficult task to determine the regularized constraint of $\boldsymbol{s}$, which is related to the motion model, and it is usually set as constant with a global motion model. If there is more complicated motion, different strategies could be adopted. Shen et al. [62] proposed a joint method combining motion estimation, object-based segmentation, and SR. This method can handle the SR problem with multiple moving objects by iteratively updating the motion fields, segmentation fields, and the HR image. He et al. [126] proposed a nonlinear least-squares technique for motion models, including both translation and rotation. Furthermore, Tian and Yap [147] proposed a method for SR with a zooming motion and employed $\|\boldsymbol{s}-\tilde{\boldsymbol{s}}\|^2$ as the PDF of $p(\boldsymbol{s})$, where $\tilde{\boldsymbol{s}}$ is the initial estimate of the motion vectors. Overall, joint super-resolution is an effective way to undertake SR without accurate registration. However, relatively complex models and extra parameters mean that the methods have not been widely applied. Of course, Bayesian methods can also prevent the propagation of estimation errors for the motion fields [53, 72].

◆ **Super-resolution without explicit motion estimation**

In recent years, SR methods without explicit motion estimation have become popular.

The motivation behind these methods is to seek an SR algorithm that is able to process sequences with a general motion pattern. Protter et al. [148] generalized the nonlocal-means (NLM) algorithm to perform SR reconstruction. Rather than calculating the data fidelity globally, the method divides both the LR images and the estimated HR image into patches to accumulate the weighted residuals of the similar patches. By constructing a penalty function combining fuzzy motion estimation and a patch-based approach, it allows the algorithm to handle diverse motion models. Following this work, Takeda et al. [54] adapted kernel regression to multi-frame SR, and this method is able to handle video sequences with general motion models. Protter and Elad [113] presented a new framework in which the pixel-wise motion field in each pair of images is replaced with a probabilistic motion field. One of the main concerns about SR methods without explicit motion estimation is the computational efficiency, since most of them adopt a patch-based manner and require iteration to obtain the final result.

3.3.2. Super-resolution without multiple low-resolution images

The goal of SR is to recover the HR details which are unobservable in the LR images. Usually, the details are recovered by combining the information across multiple LR images. However, in the real world, sufficient images with supplementary information are sometimes difficult to acquire. The performance of the reconstruction-based algorithms degrades when the magnification factor is large. Thus, researchers have turned to study SR methods for use with a single image, where the observation model

is similar to (1) as $K=1$.

Single-frame SR should not be confused with similar techniques, such as image interpolation and reconstruction methods using little extra information. The high-frequency details cannot be reconstructed without supplementary information. For example, the reconstruction-based methods [91, 149-154] involve image priors to "hallucinate" information lost during the image acquisition. Differing from the priors commonly used in multi-frame SR, the single-frame priors are typically designed to reduce edge artifacts and estimate the HR details with little additional external information. Although the edge-preserving operators can remove the ringing artifacts in image resolution enhancement, the main deficiency with mid-frequency textures prevents the methods being effective when the magnification factor is large [11]. In other words, these approaches cannot satisfy our everyday requirements, because of the limited information involved in the reconstruction model. Consequently, we do not regard traditional interpolation and reconstruction-based methods as SR in this review.

Distinguished from the traditional interpolation methods, single-frame SR learns the correspondence between the low- and high-resolution information from an external database, and thus restores the details in the HR space. As with the rapid developments in machine learning, much attention has been paid to example-based SR in recent years. The example-based algorithms [11, 12, 155-159] either exploit the internal similarities of the same image, or learn the correspondences between the LR and HR image patches from external low- and high-resolution exemplar pairs. In the

early stage, patch or feature-based approaches were used to learn the generic relationship between the LR and HR image details [12, 160, 161]. As a representative work, Freeman et al. [12] employed an MRF framework to learn the prediction from LR to HR images. However, these methods are usually computationally expensive and depend on the similarity between the training set and the test set. As a result, neighbor embedding (NE) methods and sparse coding methods have since been proposed.

The NE-based approaches assume that the small patches in the HR and LR images form similar manifolds in two distinct feature spaces [155-157, 162, 163]. Chang et al. introduced locally linear embedding (LLE) [155] to predict the HR patch as a linear combination of nearest neighbors from the training dataset, via learning the mapping relationship from the LR to HR space. In this way, the NE-based methods require fewer training samples and can be applied to a variety of images. However, the crucial problems of the NE-based methods are the blurring effects due to over- or under-fitting with the strictly fixed neighborhood size. Moreover, the LR-HR feature mappings cannot be effectively established through learning high-resolution information from the low-dimensional space.

To overcome the limitations, sparse coding (SC) approaches [11, 159, 164-166] attempt to incorporate sparse signal representation to form a learned overcomplete dictionary, and have obtained quite promising results. Supposing that the image can be represented as a sparse linear combination with an overcomplete dictionary $\boldsymbol{\psi}$ and the corresponding coefficient vector $\boldsymbol{\alpha}$ with very few nonzero entries, then the

image patch can be given as $\boldsymbol{x}=\boldsymbol{\psi}\boldsymbol{\alpha}$. In the concept of SR, for each input LR patch $\boldsymbol{y}_r$, the sparse representation will be found with respect to $\boldsymbol{\psi}_l$, and the HR patch $\boldsymbol{z}_r$ can be generated according to the HR dictionary $\boldsymbol{\psi}_h$ and the coefficients. The target is to find the sparsest representation of $\boldsymbol{\alpha}$ and the corresponding HR image by optimizing the energy function. The unified framework [11] can be interpreted as:

$$\hat{\boldsymbol{z}}=\arg\min_{\boldsymbol{z},\{\boldsymbol{\alpha}_{i,j}\}}\left\{\left\|\boldsymbol{DBz}-\boldsymbol{y}\right\|_2^2+\beta\sum_{i,j}\left\|\boldsymbol{\psi}_h\alpha_{i,j}-P_{i,j}\boldsymbol{z}\right\|_2^2+\tau U\left(\boldsymbol{z}\right)+\lambda R\left(\boldsymbol{\alpha}\right)\right\} \tag{30}$$

where $\boldsymbol{\alpha}_{i,j}$ denotes the representation coefficients for the $(i,j)th$ patch of $\boldsymbol{z}$, $\boldsymbol{\alpha}$ denotes the concatenation of all $\boldsymbol{\alpha}_{i,j}$, and $P_{i,j}$ is a projection matrix which selects the $(i,j)th$ patch from $\boldsymbol{z}$. The $U(\boldsymbol{z})$ indicates the prior term for the reconstructed image, as discussed in Section 3.2.3. By tuning λ and β, the model is able to control the tradeoff between matching the LR input and finding a HR patch which is compatible with its neighbors. In addition, τ can achieve the goal of simultaneously suppressing the noise.

The main advances since then include different training approaches for the dictionary pair [159, 166, 167], efficiency improvements [168], and various coding strategies [164, 169]. In the work of Yang et al. [11], the coefficient $\boldsymbol{\alpha}$ is assumed to be the same with respect to both the LR and HR dictionaries. However, further studies claimed that the differences and connections between the coefficients for the dictionaries should not be ignored [166, 170]. This is another tough task for single-image SR based on sparse representation. Other researchers have developed regression-based methods and some improved algorithms, such as the SR method with sparse NE [156], image SR using nonlocal autoregressive modeling [159], and

anchored neighborhood regression [171] for fast example-based SR. Recently, Dong et al. [172] presented the sparse coding based SR method, which can also be viewed as a kind of convolutional neural network with a different nonlinear mapping, and applied deep learning to learn an end-to-end mapping between the LR and HR images.

We present the experimental results of single-image SR followed by down-sampling by a scale factor of 3. Fig. 9 shows the reconstructed HR Girl images by the use of different methods. With known degradation parameters, the TV reconstruction based method [47] is effective in recovering the texture, but it generates piecewise constant block artifacts. With external information learning, all the example-based SR methods can achieve effective reconstruction results in terms of visual plausibility, and obtain sharper edges. However, the NE method [156] has a limited ability to model visually complex texture, due to its high dependency on the quality of the samples in the database. The SC [11] approach expects to learn more effective information by constructing a joint dictionary. However, it is not sufficient to use a single mapping to describe the complex relationship between different image patch pairs. Exploiting nonlocal self-similarities between patches, learning mapping functions between patches, and employing reasonable assumptions for an image can allow better image recovery, as in the ASDS-AR-NL [159] and SPM [166] methods.

Furthermore, single-frame SR offers the potential to overcome the insufficient number of LR images, and has played a significant role in some specific domains such as face hallucination [173, 174], license plate recognition [175], medical analysis

[176, 177], and satellite imaging [118], where diagnosis or analysis from few low-quality images can be extremely difficult.

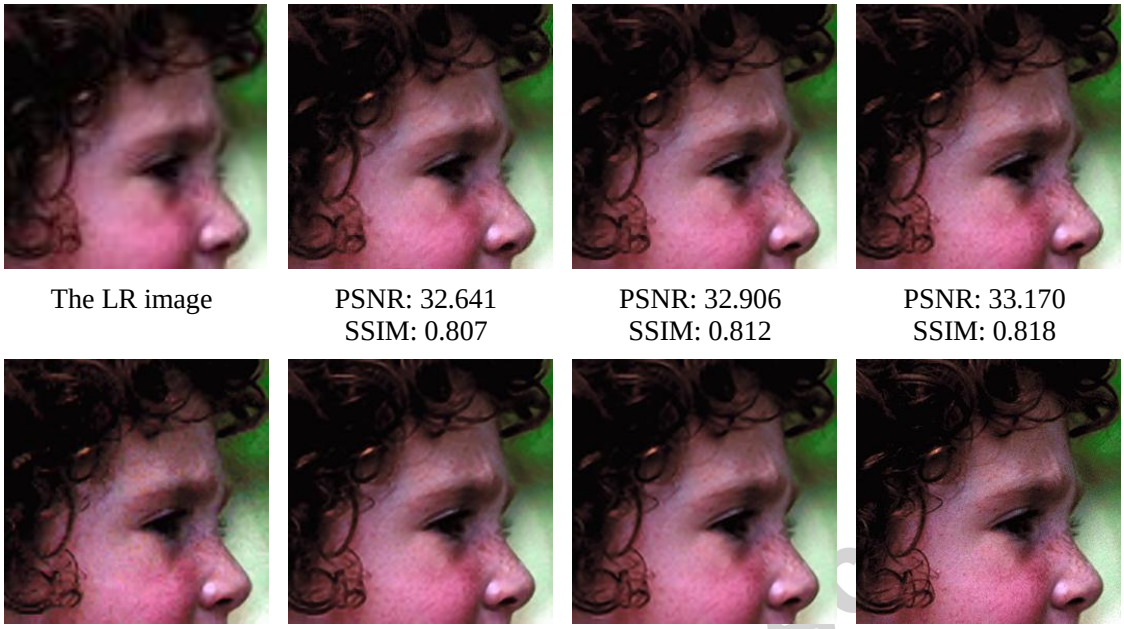

Fig. 9. Results for the Girl image with a magnification factor of 3. Top row: The LR image, NE [156], the TV-based method [47], and SC [11]. Bottom row: ASDS-AR-NL [159], SRCNN [172], SPM [166], and the original image.

3.3.3. Acceleration strategies for big data processing

There is a trend to use SR methods on large datasets, which are referred to as "big data". As a result, it is essential to develop methods that are both effective and efficient enough to satisfy the demand of the modern industrial applications.

Although abundant optimization methods have been proposed for fast SR (Section 3.2.6), the efficiency is still far away from the requirements of real-time applications. Other strategies for speed need to be developed. Zhang et al. [178] presented two methods for fast SR based on recursive multilevel reconstruction and parallel image reconstruction. It has to be mentioned that ADMM is well suited to parallelized

mechanism for solving large-scale statistical tasks. Moreover, spatially adaptive block-based methods [73, 179, 180] are commonly used approaches. However, a de-blocking process is always necessary to reduce the edge artifacts.

Alternatively, cloud computing is a simple and efficient solution, which can provide computing and storage services over the Internet [181]. Users can accomplish their goals on a very powerful computing platform employing a "super computer" [182].

4. Applications

After reviewing the methodologies above, let us return to the specific applications of SR in our daily life, which are the most basic concern. In the last three decades, various applications of SR have been addressed. In the following subsections, we give some examples of SR in the significant application fields.

4.1 Regular video information enhancement

The application of SR techniques has entered our daily life. LR video images can be converted to high-definition images using SR techniques. Hitachi Ltd. achieved the conversion of standard definition TV (SDTV) to high-definition television (HDTV) using SR technology for videos, which makes SR a particularly interesting and relevant research topic [183]. The related results can be found on the website http://www.engadget.com/2009/01/12/eyes-on-with-hitachi-super-resolution-tv/, where all the details in the frame are clearly enhanced.

Fig. 10 shows the SR results for some daily scenes. The QCIF video sequence was

processed by 3-D ISKR [1], while the Bicycle sequence was handled by the method in [73]. These typical examples show the effectiveness of SR techniques when dealing with motion outliers caused by multiple moving objects, which is common in real scenes. Furthermore, Apple Inc. announced that they have applied for a patent of SR-based optical image stabilization. SR techniques will be employed in our phones, computers, and tablets someday sooner or later.

(a) (b)

Fig. 10. The SR reconstruction of (a) a QCIF sequence [1] and (b) the Bicycle sequence [73]. The first row indicates the reference LR frames, while the second row presents the corresponding reconstruction results.

4.2 Surveillance

Nowadays, digital video recorder (DVR) devices are everywhere, and they play a significant role in applications such as traffic surveillance and security monitoring. It is, however, impossible for the moment to equip large-scale HR devices. Thus, it is necessary to study image SR techniques. Fig. 11 gives two examples of SR for the Walk sequence [184] and a UAV surveillance sequence [66]. Although the techniques have developed progressively, the practical use of video SR is still a challenge. Firstly, outdoor video devices are vulnerable to the impact of weather conditions. Moreover, video data usually feature a huge amount of data and complex motion. Some algorithms can deal with the motion outliers, but the computational efficiency limits their application. Compressed video SR has also been a focus [185, 186].

(a) (b)

Fig. 11. The SR reconstruction of the Walk sequence (top row) [184] and a UAV surveillance sequence (bottom row) [66]: (a) indicates the reference LR frames, while (b) presents the corresponding reconstruction results.

4.3 Medical diagnosis

Various medical imaging modalities can provide both anatomical information about

the human body structure and functional information. However, resolution limitations always degrade the value of medical images in the diagnosis. SR technologies have been used with the key medical imaging modalities, including magnetic resonance imaging (MRI), functional MRI (fMRI), and positron emission tomography (PET) [187]. The goal is to increase the resolution of medical images while preserving the true isotropic 3-D imaging. Medical imaging systems can be operated under highly controlled environments, and thus continuous and multi-view images can be easily acquired. Fig. 12 indicates the SR results on human brain MRI data [2] and a respiratory synchronized PET image, respectively [67].

Example-based SR for single frames has been also applied in the medical imaging field, by collecting similar images to establish a database [176, 188]. The following example presented in Fig. 13 is the reconstructed image of the single MRI image of the knee in [176]. The training database was established with a set of five standard images, including computed tomography (CT) and MRI images from various parts of the human body.

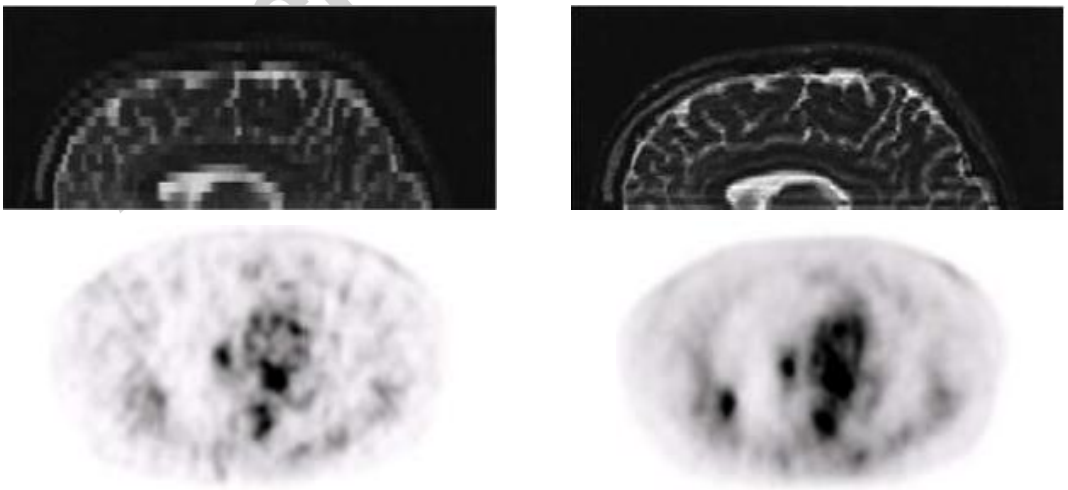

(a) (b)

Fig. 12. The SR results of (a) an MRI [2] image and (b) a PET [67] image. The first column is

the original LR images, and the second column shows the corresponding SR results.

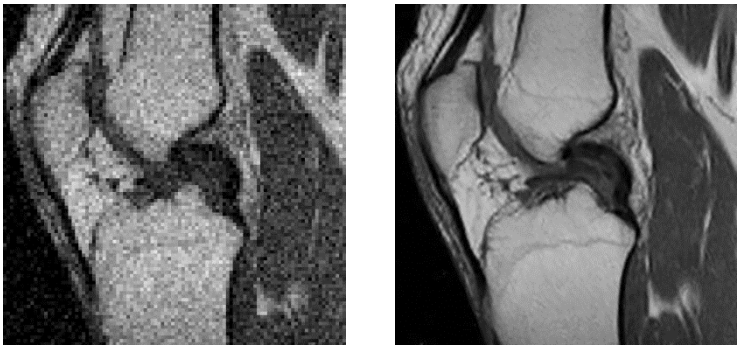

(a) (b)

Fig. 13. The single-frame SR result on the MRI knee image with a magnification factor of 4 [176]. (a) The original LR data. (b) The SR result.

4.4 Earth-observation remote sensing

As we know, the first SR idea in [31] was motivated by the requirement to improve the resolution of Landsat remote sensing images. The idea of applying SR techniques to remote sensing imaging has been developed for decades. Though data satisfying the demand for SR are not easy to obtain, there have been a few successful applicable examples for real data [25, 27, 28, 189-191]. Among them, the resolution of the panchromatic image acquired by SPOT-5 can reach 2.5 m through the SR of two 5-m images obtained by shifting a double CCD array by half a sampling interval (Fig. 3), which was the most successful case [27, 192]. In addition, Shen et al. [28] proposed a MAP algorithm and tested it with moderate-resolution imaging spectroradiometer (MODIS) remote sensing images, as shown in Fig. 14. Moreover, satellites can acquire multi-temporal or multi-view images for the same area, e.g. Landsat, CBERS, and WorldView-2, and thus provide the possibility for SR [25, 191]. An example is also given in Fig. 14, which incorporates five angular images provided by the

WorldView-2 satellite for SR [25]. SR for the spectral unmixing of fraction images has been widely studied to acquire a finer-resolution map of class labels, and is known as sub-pixel mapping [193-195]. Researchers have also attempted to apply the example-based methods to remotely-sensed image SR [196, 197].

Recently, Skybox Imaging planned to launch a group of 24 small satellites, which can provide real-time "videos" with a sub-meter resolution using SR techniques [16, 198]. At the moment, SkySat-1 and SkySat-2 have been launched and put into use. By incorporating approximately 20 frames, the ground-based distance (GSD) of the output image can be decreased to $4/5$ of the original data [16]. This is a great opportunity to bring SR techniques into our daily life.

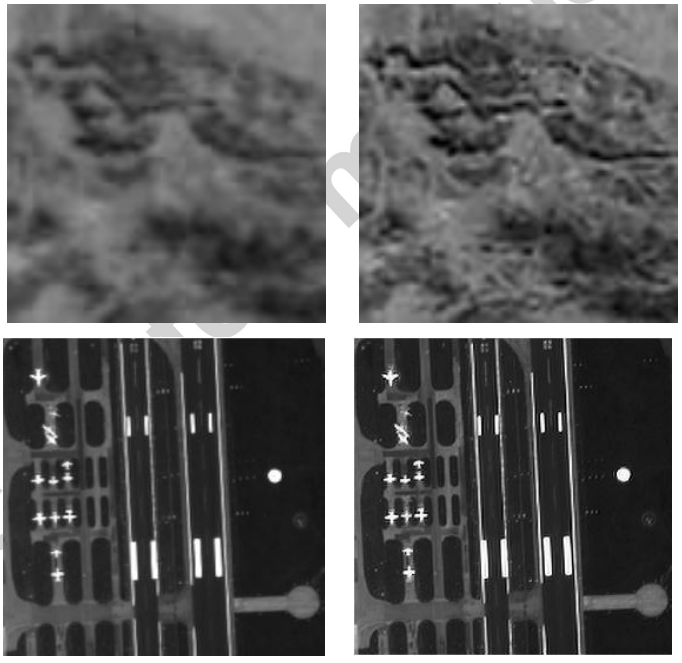

(a) (b)

Fig. 14. The SR reconstruction of remote sensing images: (a) and (b) indicate the LR and HR images, respectively. The first row shows the test on multi-temporal MODIS images with a magnification factor of 2 [28]. The second row is the SR example for multi-angle WorldView-2 images with a magnification factor of 2 [25].

The main challenges for remotely-sensed image SR are to overcome the scene

changes due to temporal differences, and to adapt the existing methods to massive amounts of observations every day.

4.5 Astronomical observation

The physical resolution of astronomical imaging devices limited by system parameters also provides a chance for SR techniques to play a role. Astronomical systems can typically collect a series of images for SR. By improving the resolution of astronomical images, SR can help astronomers with the exploration of outer space. A specific example is shown in Fig. 15 [64] showing the SR of multiple star images.

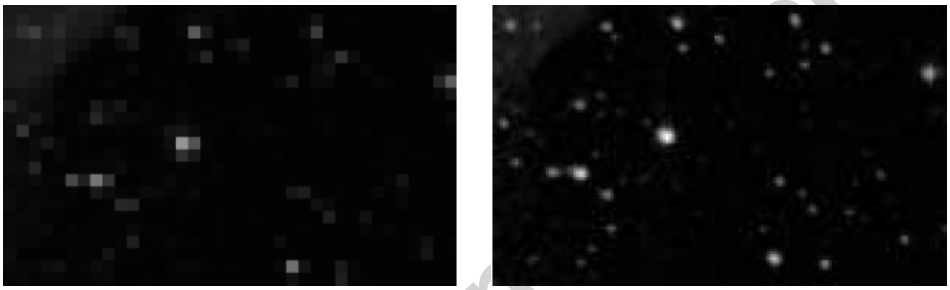

(a) (b)

Fig. 15. SR example of astronomical images: (a) the original LR image, and (b) the SR result.

Satellites are also now being sent into outer space, e.g. the lunar exploration program and the Mars Odyssey mission. Fig. 16 indicates an SR example of Chinese Chang'E-1 lunar images [199], where the result was reconstructed based on three views. The SR can enhance the image resolution, and thus improve the discernibility of small objects on the moon's surface. Beyond this, Hughes and Ramsey [200] used Thermal Emission Imaging System (THEMIS) thermal infrared and visible datasets from different spectral regions to generate an enhanced thermal infrared image of the surface of Mars.

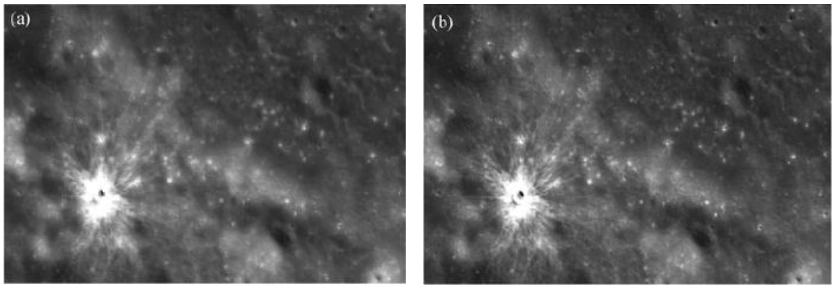

Fig. 16. The SR result of Chang'E-1 lunar images with a magnification factor of 2 [199]: (a) the original LR image, and (b) the SR result.

4.6 Biometric information identification

SR is also important in biometric recognition, including resolution enhancement for faces [24, 201, 202], fingerprints [203], and iris images [65, 204]. The resolution of biometric images is pivotal in the recognition and detection process. To deal with the LR observations, a common approach is the development of high-quality images from multiple LR images. Based on the redundancy and similarity in the structured features of biometric images, example-based single-frame SR with an external database is an effective way of resolution enhancement [11]. We give three cases of biometric image reconstruction in Fig. 17 [203, 205, 206]. Using SR, the details of the shapes and structural texture are clearly enhanced, while the global structure is effectively preserved, which can improve the recognition ability in the relevant applications.

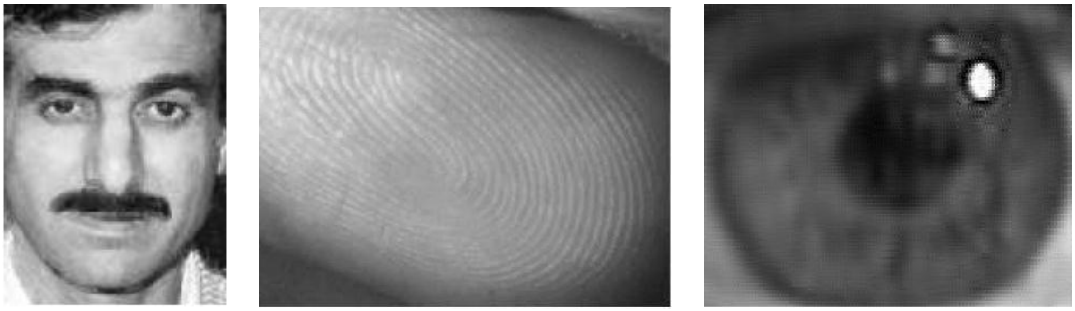

(a) (b) (c)

Fig. 17. The SR results for face [205], fingerprint [203], and iris images [189], respectively. The first row is the LR image, while the second row shows the reconstructed result. (a) Face hallucination, (b) fingerprint reconstruction, and (c) iris reconstruction.

5. Discussion and conclusions

In this article, we intended to convey the concept, development, and main applications of super-resolution (SR) over the past three decades. The main progress in SR techniques can basically be divided into three stages. In the first decade, researchers shifted their attention from the study of frequency domain methods to spatial domain algorithms. Regularized multi-frame SR framework were the main focus in the second stage. The Bayesian MAP framework became the most popular technique due to its good performance and flexible characteristics. In recent years, however, the development of multi-frame SR has slowed down, and researchers have mainly focused on SR reconstruction in the various application fields. Unfortunately, the extensive practical use of SR still remains a problem. There has been a bottleneck-style dilemma in the development of multi-frame SR, while example-based SR for single images has become a hot issue. However, the performance of these algorithms depends on the reliability of the external database.

So what should we do in further studies? More advanced, adaptive, and faster

methods with extensive applicability are always desirable. In addition, methods should be closely combined with actual requirements. The rapid development of hardware devices will also bring new challenges to the application of the SR framework. For instance, the Google Skybox project will provide us with an opportunity to obtain real-time HR "earth-observation videos" using remotely-sensed image SR. The concept of SR has also been extended to related fields such as fluorescence microscopy [17, 207-209] and multi-baseline tomographic synthetic aperture radar (SAR) imaging [210, 211]. Moreover, researchers have attempted to apply the single-frame SR techniques to the processing of medical and remote sensing imagery. However, the practicability of these methods is still limited by the time consumption, and acceleration strategies are essential for large-scale applications. In conclusion, the future of SR is still in our hands.

Acknowledgements

The authors would like to thank the editors and the anonymous reviewers for their valuable suggestions. This research is supported by National Natural Science Foundation of China (41422108), Program for Changjiang Scholars and Innovative Research Team in University (IRT1278) and National Natural Science Foundation of China (41401383).

References

[1] H. Takeda, P. Milanfar, M. Protter, et al., Super-resolution without explicit subpixel motion estimation, IEEE Transactions on Image Processing, 18 (2009) 1958-1975.

[2] H. Greenspan, Super-resolution in medical imaging, The Computer Journal, 52 (2009) 43-63.

[3] J. A. Kennedy, O. Israel, A. Frenkel, et al., Super-resolution in PET imaging, IEEE Transactions on Medical Imaging, 25 (2006) 137-147.

[4] S. C. Park, M. K. Park and M. G. Kang, Super-resolution image reconstruction: A technical overview, IEEE Signal Processing Magazine, 20 (2003) 21-36.

[5] S. Borman and R. Stevenson, "Spatial Resolution Enhancement of Low-Resolution Image Sequences: A Comprehensive Review with Directions for Future Research," Laboratory for Image and Signal Analysis (LISA), University of Notre Dame, Report, July 8 1998

[6] S. Farsiu, D. Robinson, M. Elad, et al., Advances and challenges in super-resolution, International Journal of Imaging Systems and Technology, 14 (2004) 47-57.

[7] M. Elad and A. Feuer, Super-resolution reconstruction of image sequences, IEEE Transactions on Pattern Analysis and Machine Intelligence, 21 (1999) 817-834.

[8] K. Nasrollahi and T. B. Moeslund, Super-resolution: a comprehensive survey, Machine vision and applications, 25 (2014) 1423-1468.

[9] D. Glasner, S. Bagon and M. Irani, Super-resolution from a single image, in 2009 IEEE 12th International Conference on Computer Vision, 2009, pp. 349-356.

[10] K. I. Kim and Y. Kwon, Single-image super-resolution using sparse regression and natural image prior, IEEE Transactions on Pattern Analysis and Machine Intelligence, 32 (2010) 1127-1133.

[11] J. Yang, J. Wright, T. S. Huang, et al., Image super-resolution via sparse representation, IEEE Transactions on Image Processing, 19 (2010) 2861-2873.

[12] W. T. Freeman, T. R. Jones and E. C. Pasztor, Example-based super-resolution, IEEE. Computer Graphics and Applications, 22 (2002) 56-65.

[13] D. Capel and A. Zisserman, Computer vision applied to super resolution, IEEE Signal Processing Magazine, 20 (2003) 75-86.

[14] J. Tian and K. K. Ma, A survey on super-resolution imaging, Signal, Image and Video Processing, 2011 (2011) 329-342.

[15] J. Van Ouwerkerk, Image super-resolution survey, Image and Vision Computing, 24 (2006) 1039-1052.

[16] K. Murthy, M. Shearn, B. D. Smiley, et al., SkySat-1: very high-resolution imagery from a small satellite, in Sensors, Systems, and Next-Generation Satellites XVIII, 2014, pp. 92411E-92411E-12.

[17] M. J. Rust, M. Bates and X. Zhuang, Sub-diffraction-limit imaging by stochastic optical reconstruction microscopy (STORM), Nature methods, 3 (2006) 793-796.

[18] B. Shi, H. Zhao, M. Ben-Ezra, et al., "Sub-pixel Layout for Super-Resolution with Images in the Octic Group," in Computer Vision–ECCV 2014, ed: Springer, 2014, pp. 250-264.

[19] M. Ben-Ezra, Z. Lin, B. Wilburn, et al., Penrose pixels for Super-resolution, IEEE Transactions on Pattern Analysis and Machine Intelligence, 33 (2011) 1370-1383.

[20] M. Pierre, Detection of visible photons in CCD and CMOS: A comparative view, Nuclear Instruments and Methods in Physics Research Section A: Accelerators, Spectrometers, Detectors and Associated Equipment, 504 (2003) 199-212.

[21] R. E. Coath, J. P. Crooks, A. Godbeer, et al., A low noise pixel architecture for scientific CMOS monolithic active pixel sensors, IEEE Transactions on Nuclear Science, 57 (2010) 2490-2496.

[22] M. Elad and Y. Hel-Or, A fast super-resolution reconstruction algorithm for pure translational motion and common space-invariant blur, IEEE Transactions on Image Processing, 10 (2001) 1187-1193.

[23] C. Latry and B. Rouge, Super resolution: Quincunx sampling and fusion processing, in International Geoscience and Remote Sensing Symposium (IGARSS), Toulouse, France, 2003, pp. 315-317.

[24] Y. Zhuang, J. Zhang and F. Wu, Hallucinating faces: LPH super-resolution and neighbor reconstruction for residue compensation, Pattern Recognition, 40 (2007) 3178-3194.

[25] H. Zhang, Z. Yang, L. Zhang, et al., Super-resolution reconstruction for multi-angle remote sensing images considering resolution differences, Remote Sensing, 6 (2014) 637-657.

[26] X. Zhang, E. Lam, E. Wu, et al., Application of Tikhonov regularization to super-resolution reconstruction of brain MRI images, Medical Imaging and Informatics, (2008) 51-56.

[27] H. Wang and D. Wen, The progress of sub-pixel imaging methods, in SPIE Conference Series, 2014, pp. 91420K-1.

[28] H. Shen, M. K. Ng, P. Li, et al., Super-resolution reconstruction algorithm to MODIS remote sensing images, The Computer Journal, 52 (2009) 90-100.

[29] B. Burke, P. Jorden and P. Vu, "Overview Paper-CCD Technology," in Scientific detectors for astronomy 2005, ed: Springer, 2006, pp. 225-264.

[30] J. L. Harris, Diffraction and resolving power, Journal of the Optical Society of America, 54 (1964) 931-933.

[31] R. Y. Tsai and T. S. Huang, Multi-frame image restoration and registration Advances in Computer Vision and Image Processing, 1 (1984) 317-339.

[32] D. Keren, S. Peleg and R. Brada, Image sequence enhancement using sub-pixel displacements, in Computer Society Conference on Computer Vision and Pattern Recognition, Ann Arbor, MI, USA, 1988, pp. 742-746.

[33] S. P. Kim, N. K. Bose and H. M. Valenzuela, Recursive reconstruction of high resolution image from noisy undersampled multiframes, IEEE Transactions on Acoustics, Speech, and Signal Processing, 38 (1990) 1013-1027.

[34] M. K. Ng and A. M. Yip, A fast MAP algorithm for high-resolution image reconstruction with multisensors, Multidimensional Systems and Signal Processing, 12 (2001) 143-164.

[35] N. Nguyen, P. Milanfar and G. Golub, A computationally efficient superresolution image reconstruction algorithm, IEEE Transactions on Image Processing, 10 (2001) 573-583.

[36] Y. Altunbasak, A. J. Patti and R. M. Mersereau, Super-resolution still and video reconstruction from MPEG-coded video, Circuits and Systems for Video Technology, IEEE Transactions on, 12 (2002) 217-226.

[37] S. Baker and T. Kanade, Limits on super-resolution and how to break them, IEEE Transactions on Pattern Analysis and Machine Intelligence, 24 (2002) 1167-1183.

[38] S. Lertrattanapanich and N. K. Bose, High resolution image formation from low resolution frames using Delaunay triangulation, IEEE Transactions on Image Processing, 11 (2002) 1427-1441.

[39] S. C. Park, M. G. Kang, C. A. Segall, et al., Spatially Adaptive High-Resolution Image Reconstruction of Low-Resolution DCT-Based Compressed Images, in IEEE International Conference on Image Processin Rochester, New York, 2002 pp. 861-864.

[40] S. Farsiu, D. Robinson, M. Elad, et al., Robust Shift and Add Approach to Super-Resolution,

in SPIE - The International Society for Optical Engineering, San Diego, CA, United States, 2003, pp. 121-130.

[41] R. Molina, M. Vega, J. Abad, et al., Parameter estimation in Bayesian high-resolution image reconstruction with multisensors, IEEE Transactions on Image Processing, 12 (2003) 1655-1667.

[42] T. Akgun, Y. Altunbasak and R. M. Mersereau, Superresolution reconstruction of hyperspectral images, Montreal, Que, Canada, 2004, pp. 497-500.

[43] S. Farsiu, M. D. Robinson, M. Elad, et al., Fast and robust multiframe super resolution, IEEE Transactions on Image Processing, 13 (2004) 1327-1344.

[44] M. V. Joshi, S. Chaudhuri and R. Panuganti, Super-resolution imaging: Use of zoom as a cue, Image and Vision Computing, 22 (2004) 1185-1196.

[45] C. A. Segall, A. K. Katsaggelos, R. Molina, et al., Bayesian resolution enhancement of compressed video, IEEE Transactions on Image Processing, 13 (2004) 898-910.

[46] M. K. Ng and A. C. Yau, Super-resolution image restoration from blurred low-resolution images, Journal of Mathematical Imaging and Vision, 23 (2005) 367-378.

[47] M. K. Ng, H. Shen, E. Y. Lam, et al., A total variation regularization based super-resolution reconstruction algorithm for digital video, EURASIP Journal on Advances in Signal Processing, 2007 (2007).

[48] M. Vega, J. Mateos, R. Molina, et al., Super-Resolution of Multispectral Images, The Computer Journal, 52 (2009) 153.

[49] Q. Yuan, L. Zhang, H. Shen, et al., Adaptive Multiple-Frame Image super-resolution Based on U-curve, IEEE Transactions on Image Processing, 19 (2010) 3157-3170.

[50] J. Chen, J. Nunez-Yanez and A. Achim, Video super-resolution using generalized Gaussian Markov random fields, IEEE Signal Processing Letters, 19 (2012) 63-66.

[51] H. Zhang, L. Zhang and H. Shen, A Super-resolution Reconstruction Algorithm for Hyperspectral Images, Signal Processing, 92 (2012) 2082-2096.

[52] L. Yue, H. Shen, Q. Yuan, et al., A locally adaptive L1− L2 norm for multi-frame super-resolution of images with mixed noise and outliers, Signal Processing, 105 (2014) 156-174.

[53] C. Liu and D. Sun, On Bayesian adaptive video super resolution, IEEE Transactions on Pattern Analysis and Machine Intelligence, 36 (2014) 346-360.

[54] H. Takeda, S. Farsiu and P. Milanfar, Kernel regression for image processing and reconstruction, IEEE Transactions on Image Processing, 16 (2007) 349-366.

[55] A. Tatem, H. Lewis, P. Atkinson, et al., Super-resolution land cover pattern prediction using a Hopfield neural network, Remote Sensing of Environment, 79 (2002) 1-14.

[56] M. Irani and S. Peleg, Improving resolution by image registration, CVGIP: Graphical Models and Image Processing, 53 (1991) 231-239.

[57] A. M. Tekalp, M. K. Ozkan and M. I. Sezan, High-resolution image reconstruction from lower-resolution image sequences and space-varying image restoration, in 1992 IEEE International Conference on Acoustics, Speech, and Signal Processing, 1992, pp. 169-172.

[58] R. R. Schultz and R. L. Stevenson, A Bayesian approach to image expansion for improved definition, IEEE Transactions on Image Processing, 3 (1994) 233-242.

[59] K. Aizawa, T. Komatsu and T. Saito, Acquisition of very high resolution images using stereo cameras, in Visual Communications,'91, Boston, MA, 1991, pp. 318-328.

[60] S. Rhee and M. G. Kang, Discrete cosine transform based regularized high-resolution image reconstruction algorithm, Optical Engineering, 38 (1999) 1348-1356.

[61] N. Nguyen and P. Milanfar, A wavelet-based interpolation-restoration method for superresolution (wavelet superresolution), Circuits, Systems and Signal Processing, 19 (2000) 321-338.

[62] H. Shen, L. Zhang, B. Huang, et al., A MAP approach for joint motion estimation, segmentation, and super resolution, IEEE Transactions on Image Processing, 16 (2007) 479-490.

[63] A. J. Patti, M. I. Sezan and A. M. Tekalp, High-resolution image reconstruction from a low-resolution image sequence in the presence of time-varying motion blur, in IEEE International Conference on Image Processing, Austin, TX, USA, 1994, pp. 343-347.

[64] R. M. Willett, I. Jermyn, R. D. Nowak, et al., Wavelet-Based Superresolution in Astronomy, Astronomical Data Analysis Software & Systems XIII, 314 (2004) 107.

[65] Y.-h. Li, "Robust Long Range Iris Recognition from Video Using Super Resolution," Citeseer, 2010.

[66] Y. Wang, R. Fevig and R. R. Schultz, Super-resolution mosaicking of UAV surveillance video, in 15th IEEE International Conference on Image Processing, 2008, pp. 345-348.

[67] D. Wallach, F. Lamare, G. Kontaxakis, et al., Super-resolution in respiratory synchronized positron emission tomography, IEEE Transactions on Medical Imaging, 31 (2012) 438-448.

[68] H. Zhang, L. Zhang and H. Shen, A Blind Super-Resolution Reconstruction Method Considering Image Registration Errors, International Journal of Fuzzy Systems, 17 (2015) 353-364.

[69] L. Zhang, H. Zhang, H. Shen, et al., A super-resolution reconstruction algorithm for surveillance images, Signal Processing, 90 (2010) 848-859.

[70] H. Stark and P. Oskoui, High-resolution image recovery from image plane arrays, using convex projections, Journal of the Optical Society of America A: Optics and Image Science, and Vision, 6 (1989) 1715–1726.

[71] M. Elad and A. Feuer, Restoration of a single superresolution image from several blurred, noisy, and undersampled measured images, IEEE Transactions on Image Processing, 6 (1997) 1646-1658.

[72] S. D. Babacan, R. Molina and A. K. Katsaggelos, Variational Bayesian super resolution, IEEE Transactions on Image Processing, 20 (2011) 984-999.

[73] H. Su, L. Tang, Y. Wu, et al., Spatially adaptive block-based super-resolution, IEEE Transactions on Image Processing, 21 (2012) 1031-1045.

[74] Y. Zhou, Z. Ye and Y. Xiao, A restoration algorithm for images contaminated by mixed Gaussian plus random-valued impulse noise, Journal of Visual Communication and Image Representation, 24 (2013) 283-294 http://dx.doi.org/10.1016/j.jvcir.2013.01.004.

[75] H. Shen, X. Li, Q. Cheng, et al., Missing information reconstruction of remote sensing data: A technical review, IEEE Geoscience and Remote Sensing Magazine, 3 (2015) 61-85.

[76] Y. M. Huang, M. K. Ng and Y. W. Wen, A new total variation method for multiplicative noise Removal, SIAM J. Imaging Sciences, 2 (2009) 22-40.

[77] R. Z. Shilling, T. Q. Robbie, T. Bailloeul, et al., A super-resolution framework for 3-D high-resolution and high-contrast imaging using 2-D multislice MRI, IEEE Transactions on Medical Imaging, 28 (2009) 633-644.

[78] C. Bouman and K. Sauer, A generalized Gaussian image model for edge-preserving MAP estimation, IEEE Transactions on Image Processing, 2 (1993) 296-310.

[79] E. S. Lee and M. G. Kang, Regularized adaptive high-resolution image reconstruction considering inaccurate subpixel registration, IEEE Transactions on Image Processing, 12 (2003) 826-837.

[80] A. Marquina and S. J. Osher, Image super-resolution by TV-regularization and Bregman iteration, Journal of Scientific Computing, 37 (2008) 367-382.

[81] H. Shen, L. Peng, L. Yue, et al., Adaptive Norm Selection for Regularized Image Restoration and Super-Resolution, IEEE Transactions on Cybernetics, (2015) 10.1109/TCYB.2015.2446755.

[82] H. Song, D. Zhang, P. Wang, et al., AN adaptive L 1–L 2 hybrid error model to super-resolution, in 17th IEEE International Conference on Image Processing (ICIP), 2010, pp. 2821-2824.

[83] S. Cho, J. Wang and S. Lee, Handling outliers in non-blind image deconvolution, in Computer Vision (ICCV), 2011 IEEE International Conference on, 2011, pp. 495-502.

[84] F. Suo, F. Hu and G. Zhu, Robust super-resolution reconstruction based on adaptive regularization, in International Conference on Wireless Communications and Signal Processing (WCSP), 2011, pp. 1-4.

[85] Y. Xiao, T. Zeng, J. Yu, et al., Restoration of images corrupted by mixed Gaussian-impulse noise via l 1–l 0 minimization, Pattern Recognition, 44 (2011) 1708-1720.

[86] X. Zeng and L. Yang, A robust multiframe super-resolution algorithm based on half-quadratic estimation with modified BTV regularization, Digital Signal Processing, 23 (2013) 98-109.

[87] H. Zhang, W. He, L. Zhang, et al., Hyperspectral image restoration using low-rank matrix recovery, IEEE Transactions on Geoscience and Remote Sensing, 52 (2014) 4729-4743.

[88] Z. Wang, A. C. Bovik, H. R. Sheikh, et al., Image quality assessment: from error visibility to structural similarity, IEEE Transactions on Image Processing, 13 (2004) 600-612.

[89] Q. Yuan, L. Zhang and H. Shen, Regional spatially adaptive total variation super-resolution with spatial information filtering and clustering, IEEE Transactions on Image Processing, 22 (2013) 2327-2342.

[90] L. Zhang, H. Shen, W. Gong, et al., Adjustable model-based fusion method for multispectral and panchromatic images, IEEE Transactions on Systems, Man, and Cybernetics, Part B: Cybernetics, 42 (2012) 1693-1704.

[91] J. Sun, Z. Xu and H.-Y. Shum, Image super-resolution using gradient profile prior, in IEEE Conference on Computer Vision and Pattern Recognition, 2008, pp. 1-8.

[92] M. J. Beal, "Variational algorithms for approximate Bayesian inference," University of London, 2003.

[93] S. Osher, M. Burger, D. Goldfarb, et al., An iterative regularization method for total variation-based image restoration, Multiscale Modeling and Simulation, 4 (2005) 460.

[94] Q. Yuan, L. Zhang and H. Shen, Multiframe super-resolution employing a spatially weighted total variation model, IEEE Transactions On Circuits And Systems For Video Technology, 22 (2012) 379-392.

[95] D. Bertaccini, R. Chan, S. Morigi, et al., An Adaptive Norm Algorithm for Image Restoration, Scale Space and Variational Methods in Computer Vision, (2012) 194-205.

[96] X. Li, Y. Hu, X. Gao, et al., A multi-frame image super-resolution method, Signal Processing,

90 (2010) 405-414.

[97] G. Gilboa and S. Osher, Nonlocal operators with applications to image processing, Multiscale Modeling & Simulation, 7 (2008) 1005-1028.

[98] Z. J. Xiang and P. J. Ramadge, Edge-preserving image regularization based on morphological wavelets and dyadic trees, IEEE Transactions on Image Processing, 21 (2012) 1548-1560.

[99] A. N. Tikhonov, V. I. A. Arsenin and F. John, Solutions of ill-posed problems. New York: Willey, 1977.

[100] R. C. Hardie, K. J. Barnard, J. G. Bognar, et al., High-resolution image reconstruction from a sequence of rotated and translated frames and its application to an infrared imaging system, Optical Engineering, 37 (1998) 247-260.

[101] R. Pan and S. J. Reeves, Efficient Huber-Markov edge-preserving image restoration, IEEE Transactions on Image Processing, 15 (2006) 3728-3735.

[102] T. Goldstein and S. Osher, The split Bregman method for L1-regularized problems, SIAM Journal on Imaging Sciences, 2 (2009) 323-343.

[103] L. Rudin, S. Osher and E. Fatemi, Nonlinear total variation based noise removal algorithms, Physica D, 60 (1992) 259-268.

[104] J. M. Bioucas-Dias, M. A. T. Figueiredo and J. P. Oliveira, Total Variation-Based Image Deconvolution: a Majorization-Minimization Approach, in IEEE International Conference on Acoustics, Speech and Signal Processing, 2006, pp. 861-864.

[105] M. Zhu and T. Chan, An efficient primal-dual hybrid gradient algorithm for total variation image restoration, UCLA CAM Report, (2008) 08-34.

[106] T. Chan and C. Wong, Total variation blind deconvolution, IEEE Transactions on Image Processing, 7 (1998) 370-375.

[107] Y. Dong, M. Hintermüller and M. M. Rincon-Camacho, Automated regularization parameter selection in multi-scale total variation models for image restoration, Journal of Mathematical Imaging and Vision, 40 (2011) 82-104.

[108] Q. Chen, P. Montesinos, Q. S. Sun, et al., Adaptive total variation denoising based on difference curvature, Image and Vision Computing, 28 (2010) 298-306.

[109] D. Strong and T. Chan, Edge-preserving and scale-dependent properties of total variation regularization, Inverse problems, 19 (2003) S165.

[110] H. Zou and T. Hastie, Regularization and variable selection via the elastic net, Journal of the Royal Statistical Society: Series B (Statistical Methodology), 67 (2005) 301-320.

[111] G. Steidl, S. Didas and J. Neumann, "Relations between higher order TV regularization and support vector regression," in Scale Space and PDE Methods in Computer Vision, ed: Springer, 2005, pp. 515-527.

[112] Z. Xu and E. Y. Lam, Maximum a posteriori blind image deconvolution with Huber–Markov random-field regularization, Optics letters, 34 (2009) 1453-1455.

[113] M. Protter, M. Elad, H. Takeda, et al., Generalizing the nonlocal-means to super-resolution reconstruction, IEEE Transactions on Image Processing, 18 (2009) 36-51.

[114] G. Gilboa and S. Osher, Nonlocal linear image regularization and supervised segmentation, Multiscale Modeling & Simulation, 6 (2007) 595-630.

[115] X. Zhang, M. Burger, X. Bresson, et al., Bregmanized nonlocal regularization for deconvolution and sparse reconstruction, SIAM Journal on Imaging Sciences, 3 (2010) 253-276.

[116] J. Lu, H. Zhang and Y. Sun, Video super resolution based on non-local regularization and reliable motion estimation, Signal Processing: Image Communication, 29 (2014) 514-529.

[117] T. Sasao, S. Hiura and K. Sato, Super-resolution with randomly shaped pixels and sparse regularization, in IEEE International Conference on Computational Photography (ICCP), 2013, pp. 1-11.

[118] Y. Zhao, J. Yang, Q. Zhang, et al., Hyperspectral imagery super-resolution by sparse representation and spectral regularization, EURASIP Journal on Advances in Signal Processing, 2011 (2011) 1-10.

[119] Q. Yuan, L. Zhang and H. Shen, Hyperspectral Image Denoising Employing a Spectral-spatial Adaptive Total Variation Model, IEEE Transactions on Geoscience and Remote Sensing, (2012).

[120] C. L. Lawson and R. J. Hanson, Solving least squares problems vol. 161: SIAM, 1974.

[121] P. C. Hansen and D. P. O'Leary, The use of the L-curve in the regularization of discrete ill-posed problems, SIAM Journal on Scientific Computing, 14 (1993) 1487-1503.

[122] G. H. Golub, M. Heath and G. Wahba, Generalized cross-validation as a method for choosing a good ridge parameter, Technometrics, 21 (1979) 215-223.

[123] D. Krawczyk-StańDo and M. Rudnicki, Regularization parameter selection in discrete ill-posed problems—the use of the U-curve, International Journal of Applied Mathematics and Computer Science, 17 (2007) 157-164.

[124] N. K. Bose, S. Lertrattanapanich and J. Koo, Advances in superresolution using L-curve, in IEEE International Symposium on Circuits and Systems, 2001, pp. 433-436.

[125] H. He and L. P. Kondi, A regularization framework for joint blur estimation and super-resolution of video sequences, in IEEE International Conference on Image Processing, 2005, pp. III-329-32.

[126] Y. He, K.-H. Yap, L. Chen, et al., A nonlinear least square technique for simultaneous image registration and super-resolution, IEEE Transactions on Image Processing, 16 (2007) 2830-2841.

[127] M. Seeger and D. P. Wipf, Variational Bayesian inference techniques, IEEE Signal Processing Magazine, 27 (2010) 81-91.

[128] C. Vogel and M. Oman, Iterative methods for total variation denoising, SIAM Journal on Scientific Computing 17 (1996) 227-238.

[129] P. Rodríguez and B. Wohlberg, Efficient minimization method for a generalized total variation functional, IEEE Transactions on Image Processing, 18 (2009) 322-332.

[130] P. Combettes and J.-C. Pesquet, "Proximal Splitting Methods in Signal Processing," in Fixed-Point Algorithms for Inverse Problems in Science and Engineering, H. H. Bauschke, R. S. Burachik, P. L. Combettes, et al., Eds., ed: Springer New York, 2011, pp. 185-212.

[131] S. Boyd, N. Parikh, E. Chu, et al., Distributed optimization and statistical learning via the alternating direction method of multipliers, Foundations and Trends in Machine Learning, 3 (2011) 1-122.

[132] R. Wolke and H. Schwetlick, Iteratively reweighted least squares: Algorithms, convergence analysis, and numerical comparisons, SIAM Journal on Scientific and Statistical Computing, 9 (1988) 907-921.

[133] J. Zhao, F. Shao, Y. Xu, et al., An improved Chan-Vese model without reinitialization for medical image segmentation, in 2010 3rd International Congress on Image and Signal

Processing (CISP), 2010, pp. 1317-1321.

[134] B. Wahlberg, S. Boyd, M. Annergren, et al., An ADMM algorithm for a class of total variation regularized estimation problems, arXiv preprint arXiv:1203.1828, (2012).

[135] P. L. Combettes and J.-C. Pesquet, A Douglas–Rachford splitting approach to nonsmooth convex variational signal recovery, Selected Topics in Signal Processing, IEEE Journal of, 1 (2007) 564-574.

[136] E. Esser, X. Zhang and T. F. Chan, A general framework for a class of first order primal-dual algorithms for convex optimization in imaging science, SIAM Journal on Imaging Sciences, 3 (2010) 1015-1046.

[137] L.-L. Huang, L. Xiao and Z.-H. Wei, Efficient and Effective Total Variation Image Super-Resolution: A Preconditioned Operator Splitting Approach, Mathematical Problems in Engineering, 2011 (2011) 20 10.1155/2011/380807.

[138] U. Mudenagudi, S. Banerjee and P. K. Kalra, Space-time super-resolution using graph-cut optimization, IEEE Transactions on Pattern Analysis and Machine Intelligence, 33 (2011) 995-1008.

[139] T. Tung, S. Nobuhara and T. Matsuyama, Simultaneous super-resolution and 3D video using graph-cuts, in IEEE Conference on Computer Vision and Pattern Recognition, 2008, pp. 1-8.

[140] T. Brox, A. Bruhn, N. Papenberg, et al., "High accuracy optical flow estimation based on a theory for warping," in Computer Vision-ECCV 2004, ed: Springer, 2004, pp. 25-36.

[141] G. Le Besnerais and F. Champagnat, Dense optical flow by iterative local window registration, in IEEE International Conference on Image Processing, 2005, pp. I-137-40.

[142] G. D. Hager and P. N. Belhumeur, Real-time tracking of image regions with changes in geometry and illumination, in Computer Vision and Pattern Recognition, 1996. Proceedings CVPR'96, 1996 IEEE Computer Society Conference on, 1996, pp. 403-410.

[143] L. Baboulaz and P. L. Dragotti, Exact feature extraction using finite rate of innovation principles with an application to image super-resolution, IEEE Transactions on Image Processing, 18 (2009) 281-298.

[144] H. Su, Y. Wu and J. Zhou, Super-resolution without dense flow, IEEE Transactions on Image Processing, 21 (2012) 1782-1795.

[145] H. Hu and L. P. Kondi, An image super-resolution algorithm for different error levels per frame, IEEE Transactions on Image Processing, 15 (2006) 592-603.

[146] B. C. Tom and A. K. Katsaggelos, Reconstruction of a high-resolution image by simultaneous registration, restoration, and interpolation of low-resolution images, in IEEE International Conference on Image Processing, Washington, DC, USA, 1995, pp. 539-542.

[147] Y. Tian and K.-H. Yap, Joint Image Registration and Super-Resolution From Low-Resolution Images With Zooming Motion, IEEE Transactions on Circuits and Systems for Video Technology, 23 (2013) 1224-1234.

[148] M. Protter and M. Elad, Super resolution with probabilistic motion estimation, IEEE Transactions on Image Processing, 18 (2009) 1899-1904.

[149] M. Irani and S. Peleg, Motion analysis for image enhancement: Resolution, occlusion, and transparency, Journal of Visual Communication and Image Representation, 4 (1993) 324-335.

[150] B. S. Morse and D. Schwartzwald, Image magnification using level-set reconstruction, in Proceedings of the 2001 IEEE Computer Society Conference on Computer Vision and Pattern Recognition, 2001, pp. I-333-I-340.

[151] M. F. Tappen, B. C. Russell and W. T. Freeman, Exploiting the sparse derivative prior for super-resolution and image demosaicing, in In IEEE Workshop on Statistical and Computational Theories of Vision, 2003.

[152] D. Shengyang, H. Mei, X. Wei, et al., Soft Edge Smoothness Prior for Alpha Channel Super Resolution, in IEEE Conference on Computer Vision and Pattern Recognition, 2007, pp. 1-8.

[153] M. Ben-Ezra, Z. Lin and B. Wilburn, Penrose pixels super-resolution in the detector layout domain, in IEEE 11th International Conference onComputer Vision, 2007, pp. 1-8.

[154] Y.-W. Tai, S. Liu, M. S. Brown, et al., Super resolution using edge prior and single image detail synthesis, in IEEE Conference on Computer Vision and Pattern Recognition (CVPR), 2010, pp. 2400-2407.

[155] H. Chang, D.-Y. Yeung and Y. Xiong, Super-resolution through neighbor embedding, in Proceedings of the 2004 IEEE Computer Society Conference on Computer Vision and Pattern Recognition, 2004, pp. I-I.

[156] X. Gao, K. Zhang, D. Tao, et al., Image super-resolution with sparse neighbor embedding, IEEE Transactions on Image Processing, 21 (2012) 3194-3205 10.1109/tip.2012.2190080.

[157] X. Gao, K. Zhang, D. Tao, et al., Joint learning for single-image super-resolution via a coupled constraint, IEEE Transactions on Image Processing, 21 (2012) 469-480.

[158] K. I. Kim and Y. Kwon, "Example-based learning for single-image super-resolution," in Pattern Recognition, ed: Springer, 2008, pp. 456-465.

[159] W. Dong, D. Zhang, G. Shi, et al., Image deblurring and super-resolution by adaptive sparse domain selection and adaptive regularization, IEEE Transactions on Image Processing, 20 (2011) 1838-1857.

[160] W. T. Freeman, E. C. Pasztor and O. T. Carmichael, Learning low-level vision, International Journal of Computer Vision, 40 (2000) 25-47.

[161] M. Song, D. Tao, C. Chen, et al., Color to gray: visual cue preservation, IEEE Transactions on Pattern Analysis and Machine Intelligence, 32 (2010) 1537-1552.

[162] T.-M. Chan, J. Zhang, J. Pu, et al., Neighbor embedding based super-resolution algorithm through edge detection and feature selection, Pattern Recognition Letters, 30 (2009) 494-502.

[163] K. Zhang, X. Gao, X. Li, et al., Partially supervised neighbor embedding for example-based image super-resolution, IEEE Journal of Selected Topics in Signal Processing, 5 (2011) 230-239.

[164] S. Yang, M. Wang, Y. Chen, et al., Single-image super-resolution reconstruction via learned geometric dictionaries and clustered sparse coding, IEEE Transactions on Image Processing, 21 (2012) 4016-4028.

[165] J. Yang, Z. Wang, Z. Lin, et al., Coupled dictionary training for image super-resolution, IEEE Transactions on Image Processing, 21 (2012) 3467-3478.

[166] T. Peleg and M. Elad, A statistical prediction model based on sparse representations for single image super-resolution, IEEE Transactions on Image Processing, 23 (2014) 2569-2582.

[167] K. Zhang, X. Gao, D. Tao, et al., Multi-scale dictionary for single image super-resolution, in 2012 IEEE Conference on Computer Vision and Pattern Recognition (CVPR), 2012, pp. 1114-1121.

[168] H. Zhang, Y. Zhang and T. S. Huang, Efficient sparse representation based image super resolution via dual dictionary learning, in Multimedia and Expo (ICME), 2011 IEEE International Conference on, 2011, pp. 1-6.

[169] L. Xiaoqiang, Y. Haoliang, Y. Pingkun, et al., Geometry constrained sparse coding for single image super-resolution, in 2012 IEEE Conference on Computer Vision and Pattern Recognition (CVPR), 2012, pp. 1648-1655.

[170] S. Wang, D. Zhang, Y. Liang, et al., Semi-coupled dictionary learning with applications to image super-resolution and photo-sketch synthesis, in 2012 IEEE Conference on Computer Vision and Pattern Recognition (CVPR), 2012, pp. 2216-2223.

[171] R. Timofte, V. De and L. V. Gool, Anchored neighborhood regression for fast example-based super-resolution, in 2013 IEEE International Conference on Computer Vision (ICCV), 2013, pp. 1920-1927.

[172] C. Dong, C. C. Loy, K. He, et al., "Learning a deep convolutional network for image super-resolution," in Computer Vision–ECCV 2014, ed: Springer, 2014, pp. 184-199.

[173] S. Baker and T. Kanade, Hallucinating faces, in IEEE International Conference on Automatic Face and Gesture Recognition, Grenoble, France, 2000, pp. 83-88.

[174] J. Yang, H. Tang, Y. Ma, et al., Face hallucination via sparse coding, in 15th IEEE International Conference on Image Processing, 2008, pp. 1264-1267.

[175] Y. Tian, K.-H. Yap and Y. He, Vehicle license plate super-resolution using soft learning prior, Multimedia Tools and Applications, 60 (2012) 519-535.

[176] D.-H. Trinh, M. Luong, F. Dibos, et al., Novel example-based method for super-resolution and denoising of medical images, IEEE Transactions on Image Processing, 23 (2014) 1882-1895.

[177] L. Fang, S. Li, R. P. McNabb, et al., Fast acquisition and reconstruction of optical coherence tomography images via sparse representation, IEEE Transactions on Medical Imaging, 32 (2013) 2034-2049.

[178] D. Zhang, H. Li and M. Du, Fast MAP-based multiframe super-resolution image reconstruction, Image and Vision Computing, 23 (2005) 671-679.

[179] R. S. Prendergast and T. Q. Nguyen, A block-based super-resolution for video sequences, in 15th IEEE International Conference on Image Processing, 2008, pp. 1240-1243.

[180] K. Simonyan, S. Grishin, D. Vatolin, et al., Fast video super-resolution via classification, in 15th IEEE International Conference on Image Processing, 2008, pp. 349-352.

[181] Y. S. Hu, X. Nan, P. Sengupta, et al., Accelerating 3B single-molecule super-resolution microscopy with cloud computing, Nature methods, 10 (2013) 96-97.

[182] Z. Wenwu, L. Chong, W. Jianfeng, et al., Multimedia Cloud Computing, IEEE Signal Processing Magazine, 28 (2011) 59-69 10.1109/msp.2011.940269.

[183] L. Hitachi. Super-resolution technology to convert video of various resolutions to high-definition. Available: http://www.hitachi.com/New/cnews/080924a.html, (accessed 2008.)

[184] C. Liu and D. Sun, A Bayesian approach to adaptive video super resolution, in 2011 IEEE Conference on Computer Vision and Pattern Recognition (CVPR), 2011, pp. 209-216.

[185] X. Zhang, M. Tang and R. Tong, Robust super resolution of compressed video, The Visual Computer, 28 (2012) 1167-1180.

[186] C. A. Segall, R. Molina and A. K. Katsaggelos, High-resolution images from low-resolution compressed video, IEEE Signal Processing Magazine, 20 (2003) 37-48.

[187] M. D. Robinson, S. J. Chiu, J. Lo, et al., New applications of super-resolution in medical imaging: CRC Press, 2010.

[188] Y.-H. Wang, J. Qiao, J.-B. Li, et al., Sparse representation-based MRI super-resolution

reconstruction, Measurement, 47 (2014) 946-953.

[189] M. T. Merino and J. Nunez, Super-Resolution of Remotely Sensed Images With Variable-Pixel Linear Reconstruction, IEEE Transactions on Geoscience and Remote Sensing, 45 (2007) 1446-1457.

[190] M. Elbakary and M. Alam, Superresolution construction of multispectral imagery based on local enhancement, IEEE Geoscience and Remote Sensing Letters, 5 (2008) 276-279.

[191] J. C.-W. Chan, J. Ma and F. Canters, A comparison of superresolution reconstruction methods for multi-angle CHRIS/Proba images, in SPIE Remote Sensing, 2008, pp. 710904-710904-11.

[192] K. H. Lim and L. K. Kwoh, Super-resolution for SPOT5-Beyond supermode, presented at the 30th Asian Conference on Remote Sensing 2009, Beijing, China, 2009.

[193] Y. Zhong and L. Zhang, Remote sensing image subpixel mapping based on adaptive differential evolution, IEEE Transactions on Systems, Man, and Cybernetics, Part B: Cybernetics, 42 (2012) 1306-1329.

[194] D. Vikhamar and R. Solberg, Subpixel mapping of snow cover in forests by optical remote sensing, Remote Sensing of Environment, 84 (2003) 69-82.

[195] Y. Ge, S. Li and V. C. Lakhan, Development and testing of a subpixel mapping algorithm, IEEE Transactions on Geoscience and Remote Sensing, 47 (2009) 2155-2164.

[196] R. C. Patel and M. Joshi, Super-resolution of hyperspectral images using compressive sensing based approach, ISPRS Annals of Photogrammetry Remote Sensing & Spatial Information Sciences, 7 (2012) 83-88.

[197] F. A. Mianji, Y. Zhang and Y. Gu, Resolution enhancement of hyperspectral images using a learning-based super-resolution mapping technique, in 2009 IEEE International Geoscience and Remote Sensing Symposium, 2009, pp. III-813-III-816.

[198] P. D'Angelo, G. Kuschk and P. Reinartz, EVALUATION OF SKYBOX VIDEO AND STILL IMAGE PRODUCTS, ISPRS International Archives of the Photogrammetry, Remote Sensing and Spatial Information Sciences, XL-1 (2014) 95-99.

[199] L. Li, Q. Yu, Y. Yuan, et al., Super-resolution reconstruction and higher-degree function deformation model based matching for Chang'E-1 lunar images, Science in China Series E: Technological Sciences, 52 (2009) 3468-3476.

[200] C. G. Hughes and M. S. Ramsey, Super-resolution of THEMIS thermal infrared data: Compositional relationships of surface units below the 100 meter scale on Mars, Icarus, 208 (2010) 704-720.

[201] X. Wang and X. Tang, Hallucinating face by eigentransformation, IEEE Transactions on Systems, Man, and Cybernetics, Part C: Applications and Reviews, 35 (2005) 425-434.

[202] W. Liu, D. Lin and X. Tang, Hallucinating faces: Tensorpatch super-resolution and coupled residue compensation, in IEEE Computer Society Conference on Computer Vision and Pattern Recognition, 2005, pp. 478-484.

[203] Z. Yuan, J. Wu, S.-i. Kamata, et al., Fingerprint image enhancement by super resolution with early stopping, in IEEE International Conference on Intelligent Computing and Intelligent Systems, 2009, pp. 527-531.

[204] G. Fahmy, Super-resolution construction of iris images from a visual low resolution face video, in IEEE 9th International Symposium on Signal Processing and Its Applications, 2007 ISSPA 2007, pp. 1-4.

[205] W. Liu, D. Lin and X. Tang, Hallucinating faces: Tensorpatch super-resolution and coupled

residue compensation, in Computer Vision and Pattern Recognition, 2005. CVPR 2005. IEEE Computer Society Conference on, 2005, pp. 478-484.

[206] R. Barnard, V. Pauca, T. Torgersen, et al., High-resolution iris image reconstruction from low-resolution imagery, in SPIE Optics+ Photonics, 2006, pp. 63130D-63130D-13.

[207] B. Huang, M. Bates and X. Zhuang, Super resolution fluorescence microscopy, Annual review of biochemistry, 78 (2009) 993.

[208] M. Bates, B. Huang, G. T. Dempsey, et al., Multicolor super-resolution imaging with photo-switchable fluorescent probes, Science, 317 (2007) 1749-1753.

[209] G. Shtengel, J. A. Galbraith, C. G. Galbraith, et al., Interferometric fluorescent super-resolution microscopy resolves 3D cellular ultrastructure, Proceedings of the National Academy of Sciences, 106 (2009) 3125-3130.

[210] X. X. Zhu and R. Bamler, Demonstration of super-resolution for tomographic SAR imaging in urban environment, IEEE Transactions on Geoscience and Remote Sensing, 50 (2012) 3150-3157.

[211] F. Lombardini and M. Pardini, Superresolution differential tomography: Experiments on identification of multiple scatterers in spaceborne sar data, IEEE Transactions on Geoscience and Remote Sensing, 50 (2012) 1117-1129.